A Review of Nanostructure-based Gas Sensors in a Power Consumption Perspective

Jeonghun Yun[1,*], Minkyu Cho[2,*], Kichul Lee[3], Mingu Kang[3], Inkyu Park[3,†]

[1]School of Electrical and Electronic Engineering, Nanyang Technological University, Singapore, 639798, Singapore

[2]School of Electrical and Computer Engineering, Georgia Institute of Technology, GA 30332, USA

[3]Department of Mechanical Engineering, Korea Advanced Institute of Science and Technology (KAIST), Daejeon, 34141, South Korea

[†]corresponding author

E-mail: inkyu@kaist.ac.kr (I. Park)

*equally contributed

Abstract

As the interest of personal environment and health monitoring increases, various types of gas sensors are actively researched. Traditional micro-heater based gas sensors have been improved by adopting low dimensional sensing materials such as 2-dimensional (2D) materials and nanowires. New types of sensing mechanisms such as photo-activated, photovoltaic,

triboelectric and piezoelectric approaches are also being reported. This paper introduces various types of nanostructure-based gas sensors in power consumption point of view and reviews recent progress of the nanostructure gas sensors by making comparisons between each type of gas sensor according to the sensing performance metrics such as gas response, sensitivity, response time, selectivity, resistance to interferences, manufacturing simplicity, and miniaturization.

Keywords:

Gas sensors; Nanostructures; Low power sensor; Self-powered sensor

1. Introduction

In the era of internet of things (IoT), the interests in the personal environment and health monitoring are higher than ever. In 2020, the global gas and particle sensor market was estimated as a total of $1.2B and it will be increased to $2.2B by 2026 [1]. Along with the growing gas sensor market, chemiresistive gas sensors have been researched for a long time since its first development due to the excellent gas sensing performance and low cost. Because the gas sensors used in IoT application require continuous power supply but still should satisfy the portability, low power consumption of the gas sensor is crucial.

Owing to the development of advanced nanostructure fabrication methods and sensor platform, the performance of the chemiresistive gas sensors has been progressed rapidly. To increase the gas sensitivity, various sensing materials have been suggested such as nanowires[2-4], hybrid heterojunction structures[5-8], 2-dimensional (2D) materials[9, 10], and their decoration with catalytic nanoparticles.

This review paper covers vast range of nanostructure-based gas sensors with different

working principles to explain the sensing mechanisms and introduces strategies to increase the sensor performance of each type of the gas sensor in the power consumption perspective, with their pros and cons. We focus on the gas sensors operating at power below hundred milliwatt and categorize the gas sensor into low power, ultralow power and self-powered sensors. The low power category covers the sensors with a power consumption larger than 1 mW and the ultralow power category covers the sensors with a power consumption smaller than 1 mW down to zero. The self-powered category covers the sensors that generate power while they are sensing. Through this definition, microheater-based gas sensors and self-heated multiple nanowires are classified as the low power sensors, while self-heated single nanowire, photo-activated, capacitive and colorimetric gas sensors are classified as the ultralow power sensors, and photovoltaic, triboelectric and piezoelectric gas sensors are classified as the self-powered sensors.

Table 1 shows various types of gas sensors according to their power consumptions and sensing mechanisms. The sensor performances were compared based on several performance metric such as gas response, limit of detection, response time, gas selectivity, resistance to interferences (humidity and temperature), manufacturing simplicity and miniaturization. Gas response metric indicates how many gas species can be detectable, limit of detection indicates how low gas concentration can be detected, response time indicates how fast response to gas exposure is, gas selectivity indicates how high response is for a target gas compared to other gases, resistance to interferences indicates how robust the sensor response is against external disturbances, manufacturing simplicity indicates how simple fabrication process is, and miniaturization indicates how small gas sensor can be made. The scores were given in three different levels, such as excellent, acceptable, and poor. It was hard to set more than three levels because precise performance comparison is difficult among 12 different sensing mechanisms.

For example, miniaturization scores were given because microheater-based gas sensors can be miniaturized down to a few micrometers, nanowire-based gas sensor can be smaller than a micrometer, and self-powered gas sensors require relatively much larger areas in order to harvest energy. Traditional microheater gas sensors provide excellent gas response and sensitivity, but they have the limit in miniaturization and consume relatively high power. The major source of power consumption in the conventional micro heater-based gas sensors comes from the heater design. Self-heated multiple nanowires can detect diverse gases and utilize no complicated fabrication processes, but sensitivity and selectivity are relatively poor owing to limited materials for the sensing nanowires. Calorimetric gas sensors have low resistances to interference, but can only detect few gas types, such as hydrogen and methane. By using self-heating in a smaller region such as single nanowire, the power consumption could be significantly reduced. Alternative mechanisms to the traditional heater-based gas sensors are also considered to lower the power consumption, such as photo-activated, capacitive and colorimetric approaches. Self-powered gas sensors such as photovoltaic, triboelectric and piezoelectric gas sensors use ambient energy sources such as sunlight and mechanical vibrations, but have relatively poor resistance to interference due to the susceptibility to the environmental factors.

Power consumption	Gas sensor Type	Gas response	Limit of detection	Response time	Gas selectivity	Resistance to Interference (humidity & temperature)	Manufacturing Simplicity	Miniaturization
Low Power	Microheater	O O	O O	O	O	O O	O	O
	Self-heating (multiple nanowires)	O O	O	O	O	O	O O	O
	Calorimetric	△	△	O	O	O O	O O	O
	Electrochemical	△	△	O	O O	O	O	△
Ultra Low Power	Self-Heating (single nanowire)	O	O	O O	O	O	O	O O
	Calorimetric (single nanowire)	△	△	O	-	-	O	O O
	Photo-Activated	O	O	O	O	O	O	O O
	Capacitive	O O	O O	O	△	△	O O	O O
	Colorimetric	O	O	△	O	O	O O	O
Self-Power	Photovoltaic	O	O	O	O	△	△	△
	Triboelectric	O	O	O	△	△	△	△
	Piezoelectric	△	△	O	O	△	O	△

Table 1. Performance comparison of low-power nanostructure gas sensors (OO: Excellent, O: Acceptable, Δ: Poor). The performance of each gas sensor type was evaluated based on various performance metrics such as gas response, sensitivity (limit of detection), response time, gas selectivity, resistance to interference (humidity & temperature fluctuation), manufacturing simplicity, and miniaturization.

2. Low power sensors

2.1. Semiconductor type

Metal oxide semiconductor (MOS) based gas sensors are promising owing to their simple gas sensor structures and sensing mechanisms. The sensing material needs to be heated to reduce the interfacial effect from humidity, to activate the chemisorption site for quick and high responses. The sensing material can be heated by itself or using an external heater. Herein, we discuss the power reduction techniques of MOS gas sensors using microheater platforms and self-heated nanowires.

2.1.1. Microheater platform

Typical MOS based gas sensor consists of heater, insulator, electrodes and sensing material. MEMS technology has enabled MOS based gas sensors to greatly decrease power consumption by reducing the size of a heater (Fig. 1a). The micro-heater lowers the power consumption to a few milliwatts, which is two orders of magnitude lower than that of a traditional wire heater. Due to bulky size of the wire heater and other components, the power consumption is few hundred milliwatts to few watts. Researchers have developed microheaters for more than two decades to reduce the power consumption. Throughout this effort, MEMS gas sensors using microheater platforms have been commercialized in the market. Coating of sensing materials on the microheater platforms is much more difficult than on the bulky heaters. Herein, different methods of integrating nanostructured sensing materials and microheaters to reduce the power consumption are summarized.

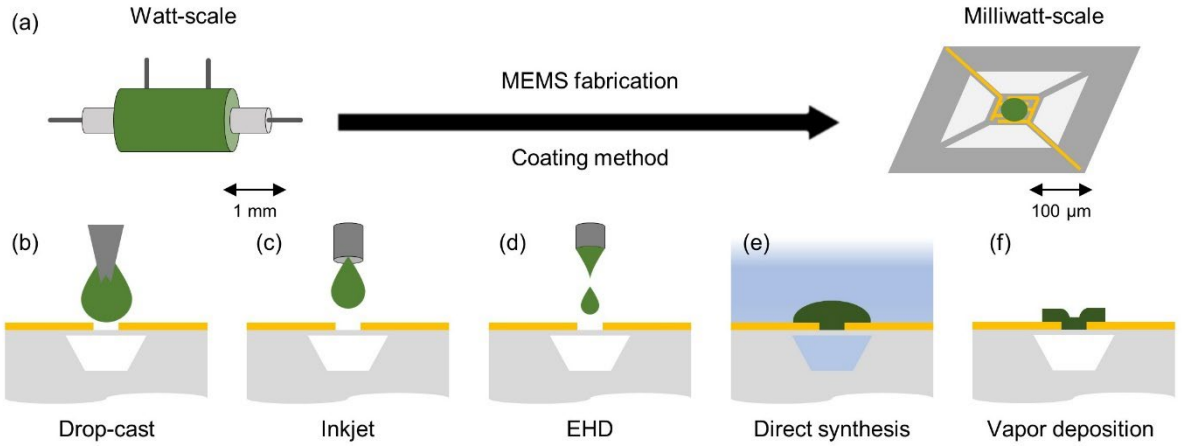

Fig. 1. (a) Power consumption of microheater based gas sensors. Power consumption can be reduced through miniaturization of gas sensors by manufacturing micro-heaters and developing coating methods.; Coating methods: (b) drop-cast, (c) inkjet printing, (d) electrohydrodynamic printing, (e) direct synthesis, and (f) vapor deposition.

The typical structure of microheater platform for MOS based MEMS gas sensors is a stacked structure of microheater, insulation layer and sensing electrodes. To reduce the heat dissipation through the substrate, the microheater is suspended from the substrate with bridges. The insulation layer electrically separates the microheater and sensing materials. The sensing electrodes are used to measure electrical conductance of the sensing material upon the exposure to gases.

There are several methods to integrate the sensing materials on microheaters, for example coating, direct synthesis, and vapor deposition. The sensing materials were synthesized by novel methods to enhance sensing behavior and coated on a microheater platform using drop-casting, ink-jetting, or electrohydrodynamic printing. Advances in the coating of sensing materials on microheater platforms have led to reductions in heater size through small coating area, which reduces the power consumption of the sensor. Sensing materials can be directly

synthesized on a microheater platform by heating within a precursor solution. Using a microheater for heating a precursor, the sensing material can be synthesized only on the microheater. Vapor deposition method along with other micromachining techniques (photolithography, etching, etc.) can also be used for the local integration of sensing materials on the microheaters.

Coating methods have been widely used because of versatility of the coating of sensing materials. Courbat et al. reported a drop-cast method for coating metal oxide on a microheater platform [11]. Tin oxide (SnO_2) with 3% palladium (Pd) paste was picked up using micro-sized glass capillaries and deposited on the interdigitated electrode using capillary forces (Fig. 1b). The droplet was 20 μm in diameter and annealed at 450 °C to sinter the material. They demonstrated carbon monoxide (CO) sensing behavior of the sensor under microheater operation. Zhou et al. reported a bridge type microheater to reduce power consumption and an exquisite drop-casting for precisely coating sensing material on the fragile structure [12]. To minimize heat dissipation through the bridge and air, the width of the bridge was narrowed from 10 μm down to 2 μm. Porous cellulose-based tips were utilized to deposit sensing material on the microheater because the structure is extremely fragile. The authors introduced a method to deposit sensing material using shadow mask deposition for mass production and multiple sensing materials in a sensor array. Unfortunately, the variation of sensing behavior among sensors and multiple gas sensor array were not investigated in this paper. The microheater can be heated to 300 °C by applying a power of 1.5 mW and hydrogen sulfide (H_2S) gas sensing response was investigated. To further reduce the power consumption, pulsed heating (1 s heating in every 6 s) was utilized. Wang et al. reported the sequential drop cast of zinc oxide nanowires and nano beta zeolites (n-BEAs) on a microheater platform to detect

hydrochlorofluorocarbon gas [13]. The catalytic effect of n-BEA with different atomic ratios of silicon and aluminum was studied and the highest sensitivity to $CHClF_2$ was observed when the atomic ratio was 20:1. The sensitivity was enhanced using multi-layer of gas sensing materials. However, these drop-casting methods are not suitable for mass production. Therefore, automatic printing methods have been utilized to deposit sensing materials on microheaters. Moon et al. reported ethanol gas sensors fabricated by an ink-jet printing method (Fig. 1c) [14]. A paste containing indium oxide (In_2O_3) nanopowders was deposited on a microheater platform by ink-jet technology and annealed using the microheater. The sensor was demonstrated to detect ethanol gas down to 0.05 ppm with an operating power of 24 mW. Kang et al. demonstrated a multiple gas sensor array fabricated by electrohydrodynamic (EHD) printing of metal oxide nanofibers (Fig. 1d) [15]. As described above, precisely controlled drop-cast and ink-jet printing techniques successfully coated sensing materials on the confined area. However, drop-cast technique is not an ideal method for mass production due to labor intensiveness, and ink-jet printing has intrinsic problems that high viscosity paste cannot be printed and the small nozzle is often clogged by the sensing material. EHD printing can pattern viscous paste in a smaller feature size than the nozzle size because the paste inside the needle is pulled out by a high electric field and concentrated at the tip of the needle by the focused electric field. The pattern size of sensing materials was around 50 μm and four different sensing materials were utilized to demonstrate a multiple sensor array within a single chip. Mixture of H_2S and nitrogen dioxide (NO_2) gases was separately identified by a principal component analysis (PCA) using the multiple sensor array. The power consumption of each microheater was 20 mW, which is not low as compared to previous papers, but this paper showed the possibility of mass production of integration of various gas sensors within a chip.

Sensing materials were directly synthesized on the microheater platforms using precursor annealing or hydrothermal reaction. Compared to coating methods, better electrical contact between sensing materials and the electrode can be obtained. Dai et al. reported the synthesis of ordered porous sensing material on a microheater using a self-assembled polystyrene bead monolayer template and precursor annealing [16]. The monolayer with 500 nm polystyrene bead was prepared by interfacial assembly and floated on a 0.1 M $SnCl_4$ precursor solution. Then, the floated monolayer was picked up with a microheater platform and the precursor solution was carried between the bead monolayer and the microheater platform by capillary force. Porous SnO_2 thin film was produced by drying and annealing the precursor. Meanwhile, the bead monolayer burned and disappeared. Gas sensing behaviors of ethanol and acetone were investigated by applying 32 mW (350 °C) to the microheater. Thanks to the formation of nano-sized SnO_2 porous thin film, it was possible to obtain fast response and high sensitivity to the target gas. The fabrication method facilitated the manufacturing of 900 sensors throughout the single fabrication because the bead monolayer can be transferred in wafer-scale. The reproducibility of five different sensors showed small sensing variation, verifying the mass production of gas sensor. However, this method is not suitable to fabricate integration of multiple gas sensor array in a single chip because of the global synthesis. Long et al. reported the synthesis of highly porous SnO_2 thin film using a microheater for annealing [17]. A SnO_2 precursor solution was drop-casted on a microheater chip and annealed by applying 12.5 mW, which heats up the microheater to ~350 °C. Since the microheater has a small thermal mass, thermal response of the microheater is very fast (~1 ms). Instantaneous heating of the micro-heater creates a highly porous structure due to the rapid evaporation of moisture inside the precursor film. Because the annealing process is carried out through the microheater, the sensing material can be deposited only on the desired microheater. This means that multi-gas

sensor arrays can be fabricated using this method. CO gas was monitored at 200 °C (7 mW), and fast response time of 9 s and recovery time of 29 s were observed. Rao et al. presented the synthesis of various metal oxide hollow sphere structures on a microheater array [18]. First, perfluorodecyltrichlorosilane was coated on the entire microheater platforms to control the wettability of the surface and thermally decomposed using a microheater where a sensing material is coated. Second, a polystyrene bead monolayer assembled using the interface method was transferred on the microheater. Due to wettability, the bead monolayer was remained only on the microheater. Then, a metal oxide precursor solution was coated on the bead monolayer by dipping into the solution and the precursor film was annealed by applying 7.5 mW to the microheater (~ 350 °C). Through this method, SnO_2, In_2O_3, nickel oxide (NiO) and SnO_2/In_2O_3 (inner/outer shell) hollow sphere arrays were fabricated. The SnO_2 nanostructure responded to formaldehyde gas at 300 °C with a heating power of 7.5 mW. However, in this paper, only the gas sensing data of the SnO_2 nanostructure were demonstrated and multiple gas sensor array was not demonstrated. Cho et al. reported the growth of zinc oxide (ZnO) nanowires and SnO_2 nanotubes on a microheater using hydrothermal reaction (Fig. 1e) [19]. The precursor for ZnO nanowires was heated by applying 45 mW to the microheater and the ZnO nanowires were locally grown on the microheater. ZnO nanowires can be used as a sensing material and also as a sacrificial structure for growing SnO_2 nanotubes. SnO_2 nanotubes were synthesized by immersing sacrificial ZnO nanowires into a SnO_2 precursor solution. Depending on the pH of the precursor solution, SnO_2 nanotubes and ZnO/SnO_2 hybrid nanostructure were obtained. The H_2S gas sensing behaviors of three nanostructures were monitored while applying 5 mW to the microheater. Xu et al. reported combination of hydrothermal growth and ink-jet printing methods to detect formaldehyde (HCHO) [20]. ZnO nanowires were grown on a microheater using hydrothermal reaction with localized ZnO seed coating and Ag@Pt core-shell

nanoparticles were loaded on the ZnO nanowires using ink-jet printing. The core-shell nanoparticle showed the highest sensitivity to HCHO when the atomic ratio of Pt and Ag was 60:40. The sensor was able to detect HCHO concentration down to 120 ppb at 280 °C with a heating power of 17 mW.

By combining a vapor deposition method and microfabrication processes, sensing materials can be selectively deposited on the microheater platform (Fig. 1f). Choi et al. reported the batch fabrication of microheater based gas sensors in 8-inch wafer-scale [21]. In the papers explained in the above paragraph, sensing materials were deposited using a separated process after the fabrication of a microheater platform. The authors showed a lift-off patterning process to precisely deposit SnO_2 thin film on a microheater platform and a xenon difluoride (XeF_2) silicon etching process to release the microheater from the silicon substrate. A SnO_2 thin film with an area of 4 μm × 8 μm was patterned, and element and morphology analyses confirmed that the XeF_2 etching did not damage the SnO_2 thin film. CO gas was detected using the fabricated sensor having a power consumption of 5 mW (~218 °C). The uniformity of the sensors in a batch was examined by measuring the resistance of the sensing material using 30 different devices and the standard deviation of the resistances was 17.4%. The repeatability and reliability test of the sensor confirmed that the sensor can measure CO gas for 100 cycles and 1000 hours of operation. Since the fabrication process is based on the photolithography, it is possible that the sensor can be made smaller to further reduce power consumption and achieve higher integration. From the same research group, the fabrication of an aligned nanowire array as a heating element of a microheater platform was reported [22]. Periodic silicon oxide nanograting was patterned on a silicon substrate by lithography, etching and oxidation processes. A nanowire structure was formed by selectively depositing a platinum (Pt) thin film

(80 nm) on the valleys of the nanograting using a sacrificial shadow deposition method. A sensing material was deposited by oblique angled deposition method on the peak of nanograting and electrically disconnected from Pt nanowires. CO gas sensing response of the sensor was characterized by applying a heating power of 4.36 mW (~500 °C). Because the thermal conductivity of nanowires is lower than that of bulk and thin film, heat dissipation through bridge was reduced, thus the power consumption of the sensor was lowered.

2.1.2. Self-heated multiple nanowires

Self-heating means direct heating of sensing materials by applying electrical power through the sensing materials. There are several advantages to use self-heating. First, power consumption can be lowered due to effective heating. In the microheater platforms, generated heat is significantly dissipated while being transferred to the sensing materials. Second, the sensor platform can be simplified because no heating element is required, but only electrodes and sensing materials are required.

Nanowire structures are promising as self-heating sensing materials because of better electrical connection and structural stability. On the other hand, the electrical connections of nanoparticles are established through many junctions between nanoparticles. This has the advantage of increasing sensitivity but makes poor electrical connections. For the thin film structure of sensing material, most of the heat can be dissipated through the substrate and the temperature of sensing material is not uniform, i.e., the center part is hotter. Herein, multiple nanowires based self-heated gas sensors are summarized.

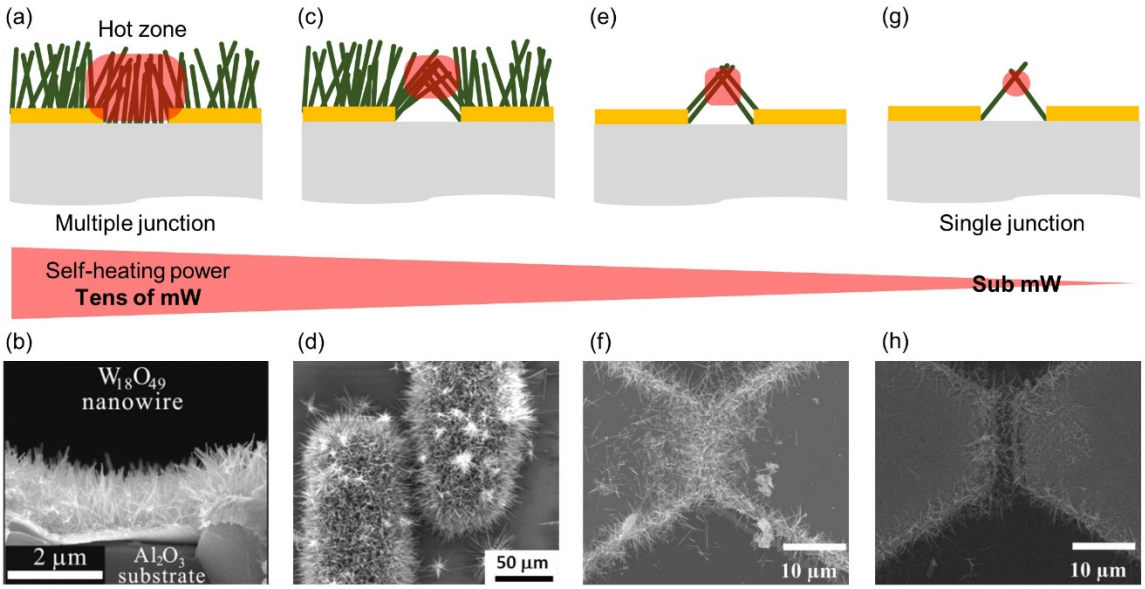

Fig. 2. Self-heating of nanowires: Nanowires grown on (a, b) electrodes and gap (Reprinted with permission from [23]), (c, d) electrodes (Reprinted with permission from [24]), (e, f) edge of electrodes, and (g, h) edge of electrodes with a few nanowires (Reprinted with permission from [25]).

Self-heating of sensing materials can heat the sensing materials effectively. Zhu et al. demonstrated a self-heating of platinum coated tungsten oxide (Pt-$W_{18}O_{49}$) nanowires for hydrogen (H_2) gas sensing (Fig. 2a, b) [23]. $W_{18}O_{49}$ nanowires were grown on the substrate using a thermal evaporation method and Pt was coated on the nanowires by sputtering. The sensor at elevated temperature (100 ~ 250 °C) using an external heater without self-heating was tested and compared with self-heated Pt-$W_{18}O_{49}$ nanowires. The kinetic responses of the sensor with self-heating power of 48 mW and external heating at 250 °C showed similar behavior. This indicates that the temperature of the self-heated sensor at 48 mW is around 250 °C. Tan et al. reported a self-heated SnO_2 nanowires for NO_2 gas sensing application [24]. SnO_2 nanowires were grown only on the electrode using a Pt catalyst layer for the vapor-liquid-

solid deposition (Fig. 2c, d). The electrical connection was built by tangling nanowires grown from interdigitated electrode. This nanowire structure can save the power consumption compared to nanowires filled in between electrodes due to low heat dissipation through the substrate. The kinetic responses of SnO_2 nanowires with self-heating and external heating to NO_2 gas were compared. When the gap between the electrodes was 30 μm, the temperature was around 250 °C by applying an electrical power of 18 mW. The power consumption can be lowered to 300 μW by reducing the electrode gap to 10 μm. From the same research group, a further low power consumption of self-heated nanowires using sparse nanowire network was demonstrated (Fig. 2e-h) [25]. SnO_2 nanowires were grown on the sidewalls of the electrodes using a catalytic chemical vapor deposition method. With different deposition times, sparse and dense nanowire networks were obtained. NO_2 gas responses of the self-heated nanowire networks were characterized, and superior gas sensing performances were observed by applying 50 μW and 1.5 mW for sparse and dense networks, respectively. Higher Joule heating power is required to heat the dense nanowire network because heat dissipation of the dense nanowire network is higher than those of the sparse nanowire network. Kim et al. reported the self-heating of gold coated ZnO nanowires for low power gas sensors [26]. ZnO nanowires were grown on the Pt electrode by the vapor-liquid-solid deposition method and gold thin layers were coated on the ZnO nanowires using sputtering. 10 nm thick gold improved the sensitivity to CO gas when a self-heating power of around 1 mW was applied. Lee et al. reported an aligned air-suspended SnO_2 nanowires array for CO gas sensing [27]. SnO_2 nanowires were formed using nanograting and angled deposition, and released from the substrate by etching silicon using XeF_2 gas. CO gas sensing performance was conducted with applying a self-heating power of 5.9 mW. Due to the C-shaped cross section of the nanowire, the nanostructure showed excellent mechanical stability under repeated self-heating.

2.2. Calorimetric type

Using this type, the gas concentration is measured by monitoring the temperature of the gas sensor while combusting the gas on the sensor. Exothermic reaction of the gas combustion generates heat, which increases the temperature of the sensor (Fig. 3a). Microheaters are promising for the calorimetric gas sensors compared to bulky heaters, such as Pt coil heater. First, as discussed in the previous section, the power consumption can be lowered. Second, if the sensor size is small and the temperature of the sensor is low (< 500 °C), convective and radiative heat transfers are minor compared to conductive heat transfer through substrate and air. This gives a linear relationship between temperature increment and combustion heat. Third, the combustion of gas effectively heats the sensor because thermal mass of the sensor is small. This causes the sensor to exhibit faster kinetic behavior.

A typical calorimetric gas sensor is composed of a microheater, a thermometer and catalyst. Compared to MOS type sensors, the microheater platform can be simplified because the sensing materials do not need to be electrically separated from the heater and connected to electrodes to measure the change in its electrical conductance. The temperature of a microheater is measured using the temperature coefficient of resistance (TCR) or Seebeck effect. Pt is widely used as a material for TCR owing to its good linearity and thermal stability. To increase the voltage of the Seebeck effect, a thermopile with thermocouples in series is used. The simplest design of the calorimetric gas sensor is composed of a microheater and catalyst since the microheater itself can be a thermometer (Fig. 3b). As similar to the microheater based MOS gas sensors, the power consumption of calorimetric gas sensors has been lowered by using novel integration methods for sensing materials. In addition, thermally stable

microheaters have been actively investigated because the operation temperatures of the calorimetric gas sensors are typically higher than those of MOS gas sensors.

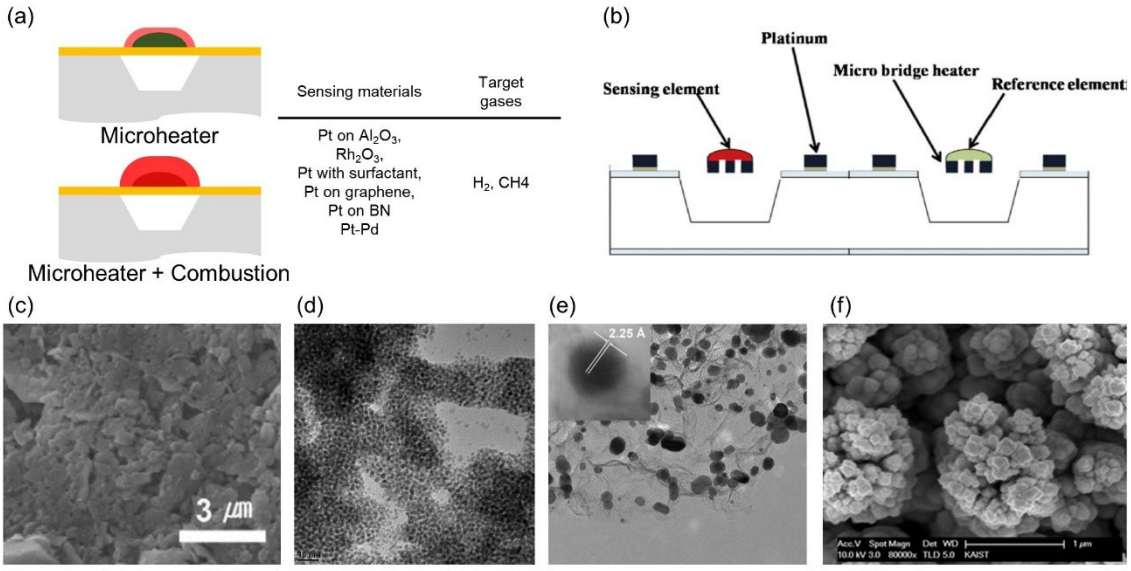

Fig. 3. Various calorimetric gas sensors: (a) Sensing mechanism and (b) structure of typical calorimetric gas sensor. Nanomaterials for calorimetric gas sensors with different Pt stabilizing methods: (c) loading on aluminum oxide nanoparticles (Reprinted with permission from [28]), (d) separating by organic ligands (Reprinted with permission from [29]), (e) loading on graphene (Reprinted with permission from [30]), and (f) hollow platinum nanostructure (Reprinted with permission from [31]).

Nanostructured sensing materials have been utilized for calorimetric sensors because the power consumption can be lowered. More catalytic reaction can occur due to large surface area of nanostructured catalyst and generates more heat. This means that calorimetric sensors with nanostructured catalyst have higher sensitivity than that with bulky catalyst. On the other hand, to obtain the same sensitivity, nanostructures catalysts require lower temperature than the bulky catalysts, which means lower power consumption for sensor operation. Although

nanostructures are utilized to enlarge the surface area of catalytic materials, their thermal stabilities are relatively poor. Therefore, catalytic nanoparticles were coated on supporting materials which are stable at high temperature. Lee at el. demonstrated calorimetric H_2 gas sensors using microheaters and Pt nanoparticle catalyst [28]. Suspended Pt microheaters with a Wheatstone configuration were fabricated by using MEMS technology and the sensing and reference materials of Pt coated alumina powders and bare alumina powders, respectively, were coated on the microheaters by drop-cast (Fig. 3c). The operation temperature of the microheater was 115 °C with the power consumption of 13.92 mW (0.5 V) and total power consumption of the four microheaters with a Wheatstone configuration was 55.68 mW (1 V). Because the resistance of Pt microheater depends linearly on the temperature with a coefficient of 3445 ppm/°C, voltage difference from the Wheatstone bridge showed a linear relationship with the H_2 gas concentration. The voltage responses to from 20 to 20000 ppm H_2 gas were 0.036 to 74.5 mV, and fast response and recovery were observed (0.36 and 1.29 s, respectively). In this paper, the Wheatstone bridge configuration was utilized to double the response and to simplify the measurement, however the power consumption quadrupled. Li et al. reported a rhodium oxide and alumina mesoporous structure for methane (CH_4) gas detection [32]. The mesoporous catalytic material was obtained by calcination of a rhodium chloride solution with mesoporous alumina colloids. The rhodium oxide/alumina hybrid and bare alumina powders were deposited on microheaters using spin-coating for sensing and reference elements, respectively. A Wheatstone bridge configuration was utilized and the microheater heated to 400 °C with a power of 25 mW. Sensing responses to 2 vol% CH_4 were observed with different rhodium/aluminum ratios for the sensing materials and the highest response was measured at the weight ratio of 4/1. The sensor showed a response time of 9 s, low variation under temperature and humidity change, and poisoning recovery from H_2S gas.

The ceramic supporting materials have relatively large thermal mass and can be a heat dissipation path. Therefore, organic molecules and 2-dimensional materials were utilized to stabilize the catalyst with small thermal mass. Brauns et al. reported Pt nanoparticles stabilized by a network of organic surfactants for a calorimetric H_2 gas sensor [33, 34]. Pt nanoparticles modified by hexadecylamine or diaminooctane were drop-casted on a microheater platform. Because of the surfactants, the catalytic reaction of Pt nanoparticles to H_2 gas at the temperature of 150 °C (20 ~ 32 mW) was well maintained. A thermopile was used to measure the temperature change of the microheater by the combustion of H_2 gas. The output voltage of the thermopile showed a good linear relationship with H_2 gas concentration. Also, a fast response was observed because of small thermal mass of the supporting material. Pranti et al. reported Pt nanoparticles with 4,4"-Diamino-pterphenyl (DATER) as a ligand for H_2 gas sensor (Fig. 3d) [29]. DATER and Pt colloidal solutions were consecutively dropped on a microheater platform. The sensor was heated at 90-130 °C by applying power of 14-45 mW and the difference of output voltages between thermopiles at reference and catalyst coated microheaters was measured. DATER ligand showed more consistent response than other ligands. Harley-Trochimczyk et al. employed Pt coated graphene aerogel and a polysilicon microheater for detecting H_2 gas (Fig. 3e) [30]. Polysilicon was adopted for the heating element because of its robustness against electromigration. Pt coated graphene aerogel was prepared using freeze dry of graphene aerogel immersed in a chloroplatinic acid solution followed by annealing and was drop-casted on the microheater. Graphene supporting structure was thermally stable compared to surfactant molecular structure as well as small thermal mass and large surface area. The sensor was tested at 320 °C with a power of 11 mW and the response time to H_2 gas was shorter than 1 s. Pulse measurement decreased the power consumption to 2.2 mW without sacrificing the response. However, because polysilicon has lower temperature coefficient of resistance

compared to Pt, the sensitivity was lower. The same research group demonstrated a silicon carbide microheater for a stable high-temperature calorimetric gas sensor [35]. Employing polysilicon as a heating element improved the stability of the sensor, however polysilicon is still not stable at high temperature (~ 500 °C) due to recrystallization. Silicon carbide is robust at high temperature as well as manufacturable by microfabrication. Pt loaded boron nitride aerogel was used as a catalyst material because of superior thermal stability of boron nitride that graphene does not have. The sensor was characterized to propane gas at 500 °C with a power of 20 mW and the resistance of the silicon carbide microheater showed minor drift for 100 h. Non-linear behavior of resistance change upon propane concentration was observed due to the mass transfer limit of propane at 500 °C and repeatable response was observed over 36 h. Since the silicon carbide has small negative temperature coefficient, the resistance change was -1.7% when exposing 2% propane. 10% duty cycle was demonstrated to reduce the power consumption and showed consistent response to sensor with a continuous heating.

Direct growth of catalytic materials can improve the thermal conduction between catalyst and microheater. Karpov et al. developed the Pt and Pd coated porous alumina membrane, which is a supporting layer for microheater in a calorimetric CH_4 gas sensor [36]. Microheaters were fabricated on a porous alumina membrane, and Pt and Pd nanoparticles were synthesized by drop casting of a precursor solution followed by annealing. They demonstrated the differential method composed of measurement at two different temperatures (around 200 °C and 450 °C) can reduce the power consumption by eliminating reference microheaters. At the low temperature, the sensor response was influenced by environment factors such as humidity and temperature, but not by combustion of CH_4. At the high temperature, the sensor response was influenced by both the environment factors and the combustion of CH_4. By measuring the

difference between two sensor responses at the high and low temperatures, environment effects can be eliminated. Several voltage pulses were applied to the microheater in a special sequence within 660 ms. Because the sensor utilized pulse heating mode, the power consumption could be lowered to 1.18 mW when measuring twice per minute, which is equivalent to 2.2% duty cycle. Orbe et al. developed a calorimetric H_2 gas sensor using porous Pt nanostructure grown using an electrodeposition method [37]. The electrodeposition enabled a direct and localized integration of sensing material on the microheater, which lowered the power consumption. The H_2 gas response of the sensor was characterized at 220 °C with a power of 8 mW and an increase in resistance of 1.2% was observed when 1.6% H_2 gas (40% of the lower explosive limit) mixed in the air was exposed. The reference microheater without a sensing material showed a decrease in resistance by 0.1% because of the high thermal conductivity of H_2 gas. The high response was enabled by good thermal conduction between the sensing material and the heater. The same research group reported a local growth of hollow Pt nanostructures for a calorimetric H_2 gas sensor (Fig. 3f) [31]. First, ZnO microrods were grown on a microheater platform using a hydrothermal method and then Pt nanostructure was formed on the microrods by dissolving ZnO in a Pt precursor solution. The sensor with applying a power of 4 mW (72 °C) showed 0.77% increase in resistance when 1.6% H_2 gas was exposed. The local growth of the sensing material allowed to lower the power consumption. Since the sensing mechanism uses heat from combustion, most calorimetric sensors have been demonstrated to measure CH_4 and H_2 gases with high heat of combustion. Although design of high-performance catalyst should be further required to enhancing the gas selectivity, calorimetric gas sensors are promising because of their simple structure and sensing mechanism.

2.3. Electrochemical type

By reducing the size, power consumption of the electrochemical sensor can be reduced. However, miniaturization of the electrochemical sensor is still challenging because it is difficult to fabricate an appropriate reference electrode, which can provide constant potential in various gases. The development strategy of electrochemical gas sensors is to make a room temperature gas sensor by applying a polymer electrolyte that operates at room temperature and electrodes with high selectivity. However, it is difficult to scale down these room temperature electrochemical gas sensors because of the difficulty in microfabrication of polymer. Here, we introduce a paper that developed a micro-size sensor equipped with a microheater.

Lee et al. developed microscale electrochemical cell for carbon dioxide (CO_2) gas sensors [38]. The structure of microheater is similar as that of microheater for MOS type gas sensors. The microheater was suspended from the substrate and covered with a silicon dioxide layer to electrically insulate the microheater. The electrochemical cell, composed of Pt electrode, sensing material (Li_2CO_3), electrolyte (Li_3PO_4), reference electrode (not stated in the paper) and Pt electrode, was mounted on a microheater. The cell used Li-ion as a charge carrier in the electrolyte and had to be heated to activate the electrolyte for providing sufficient ion conductivity of Li ions. In this sensor, the microheater heated the electrochemical cell with a power of 59 mW. Electromotive force (EMF) to different CO_2 gas concentrations showed Nernstian behavior with a slope of 50.5 mV/dec and the selectivity to hydrocarbon gases was characterized. However, the sensor fabrication needs to be optimized because the measured Nernstian slope is lower than the theoretical value and the power consumption is higher than other microheater based gas sensors.

3. Ultralow power sensors

3.1. Semiconductor type (self-heated single nanowire)

Unlike self-heated multiple nanowires, the self-heating of a single nanowire can lower power consumption down to microwatts (Fig. 4a). Heat capacity and heat dissipation of individual nanowire is much smaller than that of multiple nanowires. In addition, low heat dissipation using suspended nanowire and low thermal conductivity of nanowire further reduces the power consumption. Herein, the fabrication of nanowires for self-heated gas sensor applications are summarized.

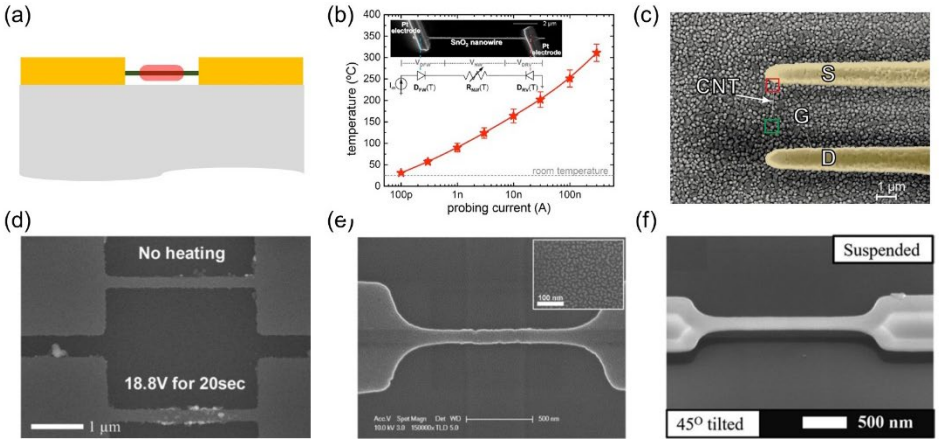

Fig. 4. Various self-heating single nanowire gas sensors: (a) Hot zone of self-heated single nanowire, (b) SnO_2 nanowire (Reprinted with permission from [39]), (c) carbon nanotube (Reprinted with permission from [40]), (d) selective Pd coated silicon nanowire (Reprinted with permission from [41]), (e) Pd coated silicon nanowire (Reprinted with permission from [42]), (f) suspended Pd coated silicon nanowire (Reprinted with permission from [43]).

In the early days, transferring a nanowire from a growing substrate to the device substrate was utilized to fabricate single nanowire-based gas sensors. Prades et al. reported self-heating of SnO_2 nanowire for NO_2 gas sensing (Fig. 4b) [39]. SnO_2 nanowires synthesized by a CVD

method were transferred to a suspended silicon membrane substrate and individually connected to Pt electrodes by the focused ion beam induced deposition of Pt. Gas responses of SnO_2 nanowire heated by self-heating and an external heater were measured, and it was confirmed that the self-heating of the nanowire does not degrade the performance of gas sensing. Also, the temperature of self-heated nanowire could be estimated by comparing the response of nanowire heated by an external heater. The optimized self-heating power was lower than 27 μW (~270 °C). Chikkadi et al. developed a suspended carbon nanotube (CNT) sensor for NO_2 detection with a short recovery time using self-heating (Fig. 4c) [40]. A CNT was transferred to predefined Pd electrodes with a gap of 3.6 μm. The CNT showed 90% current response to 900 ppb NO_2 gas and the self-heating of the CNT was utilized to accelerate the recovery by increasing temperature with applying a self-heating power of 2.6 μW for 10 min. In this paper, the self-heating was not utilized to accelerate the response of the sensor, which is thought to be due to the large electrical noise during self-heating comparable to the gas sensing response.

The nanowire transfer is a versatile method for fabricating single nanowire-based gas sensors using nanowires of various materials. However, this process is not suitable for mass production. Thus, single nanowire devices fabricated using top-down processes have been utilized for self-heated nanowire gas sensors. Yun et al. demonstrated selective functionalization of silicon nanowires using self-heating for H_2 gas sensing (Fig. 4d) [41]. Silicon nanowires were fabricated by electron beam lithography followed by reactive ion etching. Pd nanoparticles were coated on the nanowires using local hydrothermal reaction with a Pd precursor solution and local polymer decomposition with Pd evaporation. Local hot zone generated by self-heating of a silicon nanowire enabled localized Pd coating on the silicon nanowire. Self-heating of a Pd coated silicon nanowire reduced the response and recovery times to H_2 gas, however

response was reduced together because the hydrogen solubility in Pd is lowered at the high temperature. Even though the response of the sensor is lowered, fast response and recovery times were important to early detection of gas. The nanowire with applying 360 μW showed a response of 106% to 0.5% H_2 gas and a response time of 24 s. Ahn et al. reported a self-heated Pd coated silicon nanowire for H_2 gas sensing (Fig. 4e) [42]. Silicon nanowires were fabricated by complementary metal oxide semiconductor compatible processes and Pd (thickness ~1 nm) was deposited using a physical vapor deposition method. Dimension of the nanowire was a length of 1 μm (channel), a width of 110 nm, and a thickness of 40 nm. The nanowire pattern was obtained by deep ultraviolet lithography and photoresist ashing. Moderate doping concentration of the channel region was used to lower the applied voltage of self-heating by lowering resistance of the nanowire, and to reduce the variation of self-heating power while exposing H_2 gas even though the sensitivity decreased. H_2 gas response of the sensor was characterized while applying a constant voltage of 1.7 V (74.2 μW) and 1.7% response to 1% H_2 gas was observed. In terms of the heating power, the self-heating power was changed 1.7% when exposed to H_2 gas, however it is much smaller than other self-heated gas sensors because of the moderate doping concentration. Self-heating of the nanowire enhanced the gas selectivity, reduced response and recovery times, and suppressed the effects to interfering environment, such as humidity and CO that hinder the Pd-H_2 reaction. Afshar et al. reported a self-heated indium-tin-oxide (ITO) nanowire for NO_2 gas sensor [44]. An ITO nanowire with a width of 350 nm and a length of 90 μm was fabricated by laser annealing of an amorphous ITO thin film followed by HCl etching. NO_2 gas sensing behavior was tested with a constant self-heating power of 3.93 mW (~ 160 °C). Even though the self-heating of the ITO nanowire was utilized, the power consumption was high because the nanowire was long. Seo et al. reported a Pd coated suspended carbon nanowire for H_2 gas sensor [2]. Suspended carbon nanowire anchored by

carbon posts was fabricated by two successive UV lithography steps for patterning posts and microwire followed by pyrolysis of the photoresist. After pyrolysis, the micro-size photoresist was shrunk to a carbon nanowire with a diameter of 200 nm. Pd nanoparticles were deposited on the carbon wires by electrodeposition method. They demonstrated self-heating for accelerating the recovery of the sensor, but not for accelerating the response of the gas. Therefore, power consumption was 6.25 nW for gas measurement and around 30 μW for recovery. However, in practical application, this scenario is not applicable because when the target gas is removed cannot be predicted. Yun et al. developed a suspended silicon nanowire coated with Pd for H_2 gas sensor (Fig. 4f) [43]. Suspended silicon nanowires reduced power consumption by 75% as compared to non-suspended silicon nanowires. The response to H_2 gas with a self-heating power of 41-147 μW was measured. Self-heating of the Pd-coated silicon nanowires increased the sensitivity by a factor of 1.21, which differs from the typical behaviors of Pd-based H_2 gas sensors. The self-heated Pd-silicon nanowire can improve not only response and recovery times, but also sensitivity. Moreover, CO and humidity effects on the sensor were also reduced by self-heating. Self-heated single nanowire gas sensors are promising for mobile devices powered by limited electrical power supply because of ultralow power consumption. However, gas sensors fabricated by transfer methods are unavoidably subject to large deviations from sensor to sensor, and gas sensors fabricated by top-down fabrication processes can use only limited material types. To put the self-heated nanowire-based gas sensor to practical use, it is necessary to develop an advanced nanowire manufacturing process that can be mass-produced and reproducible using a variety of materials.

3.2 Calorimetric type

Microheater based calorimetric gas sensors used supporting materials for stabilizing catalytic materials. However, in a nanowire heater, coating stabilized catalytic materials is impossible because of small size. Zhang et al. reported the self-heating of a Pt coated silicon nanowire for calorimetric acetone gas sensor [4]. Pt catalyst for burning acetone was directly coated on the silicon nanowire. A heating power of around 1 mW was applied to the Pt coated nanowire and the electrical current of the Pt coated nanowire was changed while exposing 20% acetone mixture. Ultralow power calorimetric gas sensors have not been widely demonstrated due to the difficult fabrication processes and the inability to fabricate effective catalyst.

3.3. Photo-activated type

The effect of light irradiation on the gas sensor material has known to help the absorption and desorption of target gases. The principle of photo-activated gas sensors relies on the mechanism of electron-hole pair generation through the light irradiation, and the involvement of the generated carriers to form oxygen species to facilitate the absorption and desorption of gas molecules (Fig. 5a). More detailed review papers on light-activated gas sensors have been published earlier [45]. For the light source of the gas sensor, single photon energy above the bandgap of the sensing material is required to maximize the generation of free carriers. Various light-activated sensing materials such as metal oxides, reduced graphene oxide, transition metal dichalcogenide materials have been utilized. The sensing materials for the light-activated gas sensor are functionalized with other materials to enhance the light absorption. Sabri et al. demonstrated soot template visible-blind TiO_2 fractals as a photoactive gas sensor to detect acetone [46] (Fig. 5b). The sensor had ~ 3 times the response when under UV light as compared to the dark conditions. Metal nanoparticle-decorated (e.g. Au [37, 38] and Pt [39]) metal oxide

gas sensors were reported for room temperature photo-activated room-temperature gas sensing (Fig. 5c). Heterojunction photo-activated gas sensors have been reported with the enhanced response to interact with target gases under light illumination. The use of the heterojunction in photo-activated type gas sensors is to take advantages of both material characteristics; A material that can affectively absorb the photon energy while the other can effectively interact with the target gas. Han et al. exhibited In_2O_3-sensitized ZnO nanoflower gas sensor for formaldehyde detection. The sensor shows up to 419% response to 100 ppm formaldehyde under visible light (λ=460 nm) irradiation (Fig. 5d) [47]. Park et al. reported UV-enhanced SnO_2-core/ZnO shell nanowire structure for NO_2 detection. The SnO_2-core/ZnO_2-shell nanowires showed 2-3 and 2-6 folds increased response to NO_2, respectively, as compared to the pristine SnO_2 and ZnO_2 nanowires [5]. Xenon light source is very common for the light-enhanced gas sensor due to its high optical output power and wide wavelength spectrum. However, the lamp is bulky and consumes high power. Energy-efficient light source such light emitting diode (LED) allows a development of low-power light-enhanced gas sensor. Cho, et al. demonstrated light-enhanced ZnO nanowire gas sensor integrated with 390 nm micro-LED. The sensor showed response to NO_2 with power consumption less than 1 mW (Fig. 5e) [48]. Li et al. reported visible light assisted NO_2 gas sensor using CdS nanoflakes. Attributed to the low bandgap of CdS (2.4 eV), the sensor response could be enhanced with a green light LED illumination [49]. The lower limit of detection was as low as 100 ppb. Jo et al. demonstrated UV-enhanced TiO_2 sensor coated with mixed matrix membrane (MMM) composed of zeolitic imidazole framework (ZIF-7) nanoparticles and polymers. The sensor was able to detect 5 ppm formaldehyde at room temperature removing ethanol interference by the molecular sieving of MMM (Fig. 5f) [50]. Another work in the same group demonstrated the hybrids of $Cu_3(HHTP)_2$ (HHTP = 2,3,6,7,10,11-hexahydroxytriphenylene) nanoflakes and Fe_2O_3 nanoparticles [6] that

enhanced the hole carrier lifetime enabling highly sensitive and reversible NO_2 detection.

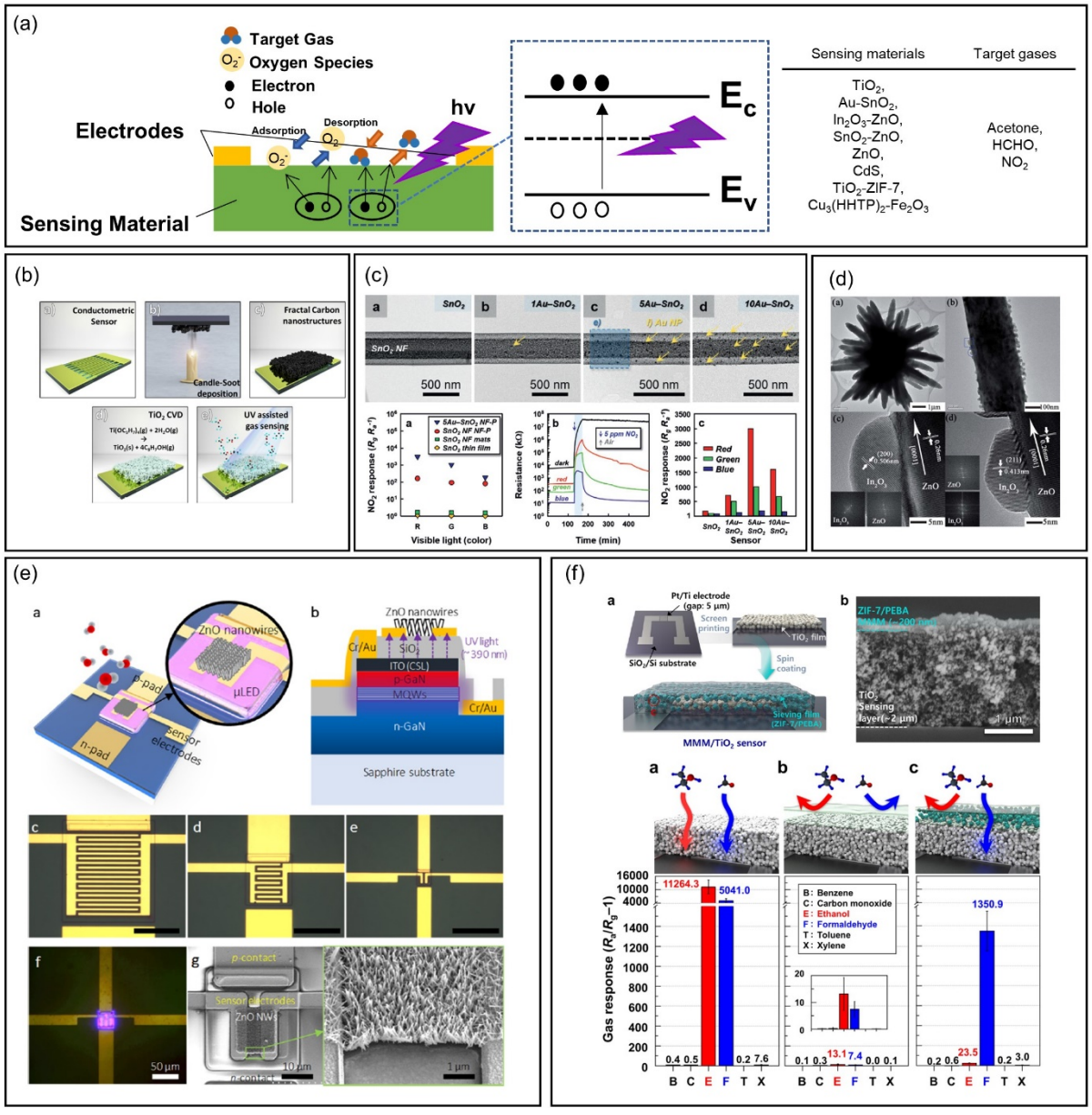

Fig. 5. Various photo-activated gas sensors: (a) Illustrations of photo-activated gas sensors. (b) Fabrication process of soot template visible-blind TiO_2 photoactive gas sensor (Reprinted with permission from [46]). (c) TEM images of SnO_2 nanofiber with different plasmonic Au nanoparticle concentration and the sensor response to NO_2 under illuminations with various

wavelengths (red, green and blue) of light [51]. (d) TEM images of InO_2-sensitized ZnO nanoflower (Reprinted with permission from [47]). (e) Schematic illustrations, optical microscope and SEM images of the photo-activated gas sensor on a micro LED (Reprinted with permission from [48]). (f) UV-enhanced TiO_2 coated with mixed matrix membrane (ZIF-7/PEBA) showing high formaldehyde gas selectivity (Reprinted with permission from [50]).

3.4. Capacitive type

The capacitive gas sensor relies on the capacitance change of the sensor during the gas absorption. It has advantages for having a simple structure, easy miniaturization and ability to be integrated with a sensing circuitry. In case of simple parallel electrode pair configuration, the basic sensing mechanism could be described by the following formula:

$$C = \varepsilon_r \varepsilon_o \frac{A}{d}$$

where, ε_r is relative permittivity, $\varepsilon_o$is vacuum permittivity, A is the electrode area, and d is the distance between two electrodes. For the gas sensor, the changes of either ε_r or d are translated into the capacitance change upon the gas absorption (Fig. 6a). It is reported that most capacitive sensing mechanism is by the change of d upon gas absorption because most of the target gases have similar permittivity. The capacitive sensor electrodes are either interdigitated electrode pair or parallel plates. The interdigitated electrodes are convenient for the dispensing of sensing materials, but has smaller capacitance than the parallel plate configuration. The parallel plate type capacitive gas sensor has advantages of achieving high capacitance due to large electrode area. Zeinali et al. investigated the performance comparisons of parallel and interdigitated capacitive sensors based on Cu-BTC (copper-benzene-1, 3, 5-tricarboxylate) [52].

They found that the parallel plate electrode has higher gas sensitivity while the interdigitated electrode results in shorter recovery time, better repeatability, and easier reproducibility (Fig. 6b). The sensing materials for the capacitive sensors are required to have high surface-area-to-volume ratio (SVR) with an ability to absorb/desorb target gases. The sensing materials are mostly molecular sieves, metal oxides, and metal organic frame frameworks (MOFs). Recently, MOFs have been researched actively for the capacitive sensor applications (Fig. 6c) [53]. Andres et al. reported the MIL-96(Al) MOF thin film-based capacitive via the Langmuir−Blodgett (LB) method [54]. They found that the sensors are highly responsive to other volatile compounds and relevant gases. Most of the MOF capacitive type sensor is susceptible to high humidity at room temperature [53]. However, Assen et al. demonstrated a capacitive NH_3 sensor based on a rare-earth (RE) MOF (RE-fcu-MOF) showing minor change of the sensing signal with relative humidity (RH) ranging from 5 – 85% (Fig. 6d) [55], although the paper did not explain why it has such good resistance to humidity change. For H_2 detection, Yamazaki et al, demonstrated Pd-based MEMS capacitive sensor that has an inverted T-shaped electrode and a ring-shaped Pd alloy ($Pd_{78}Cu_5Si_{17}$) layer. The deformation of the Pd alloy structure changes the capacitance underneath by physically pressing a spring-loaded capacitance plate. The sensor showed excellent gas selectivity against CH_4, CO_2, and He (Fig. 6e) [56].

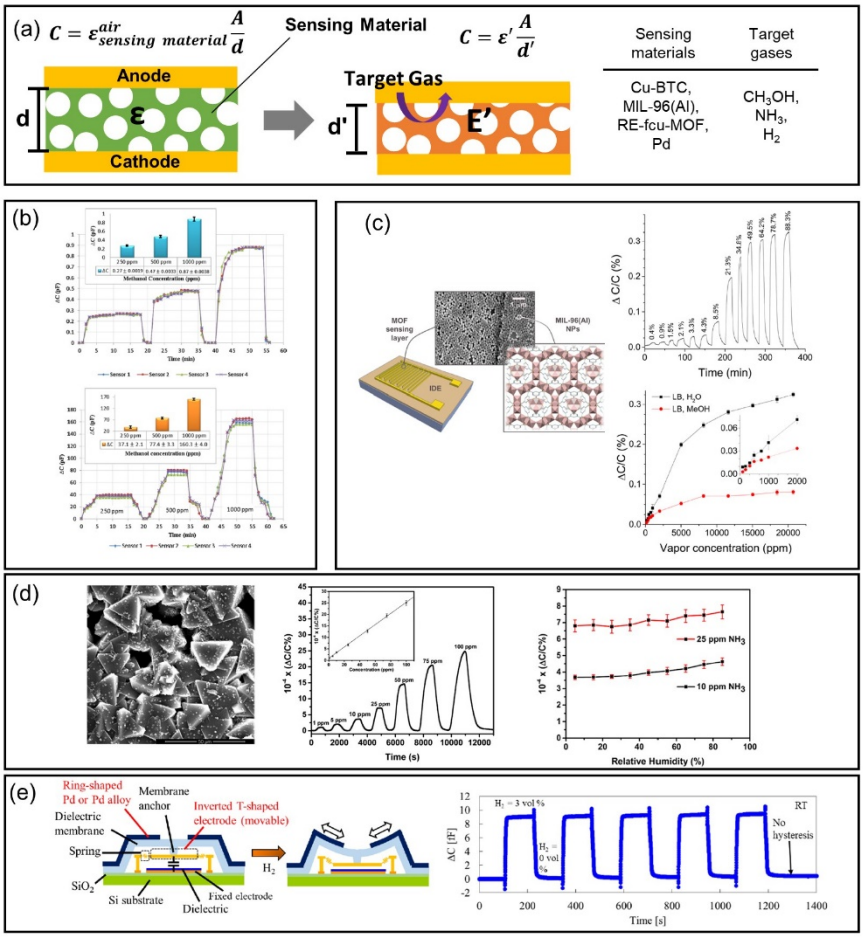

Fig. 6. Various capacitive gas sensors: (a) Illustrations of capacitive gas sensors. (b) The comparison between interdigitated and parallel capacitive sensors for methanol detection (Reprinted with permission from [52]). (c) MIL-96(Al) MOF thin film-based capacitive humidity sensor (Reprinted with permission from [53]). (d) A SEM picture and NH_3 sensing characteristics of the capacitive NH_3 sensor based on a RE-fcu-MOF (Reprinted with permission from [55]). (e) A schematic illustration of Pd-based MEMS capacitive H_2 sensor and the sensor response to 3% H_2 (Reprinted with permission from [56]).

3.5 Colorimetric type

The colorimetric sensors are well known in analytical chemistry. Most of the reported colorimetric sensor uses chemical reaction to the gas analyte and the reaction is translated into the color spectral change shown Fig. 7a. Some of the sensing probes use lock-and-key approach which responds only to a specific target gas. Other uses an array of sensing materials, and each sensing material in the array response to gases in different degree. To amplify the response to the target gases, these sensing materials are dispensed in forms of structures with high SVR, such as nanofibers, membranes. The most common technique is electrospinning that uses electric forces to draw charged polymer solutions out of a nozzle forming fibers with hundreds of nanometers in diameter [57-61]. Other techniques coat sensing materials on high SVR nanostructures. There are various nanostructure platforms reported for the colorimetric gas sensors, such as nanowires, yarn (Fig. 7b) [62], and textile (Fig. 7c) [63] and porous structure (Fig. 7d) [64]. Wang et al. showed a colorimetric sensor based on methyl yellow-impregnated electro-spinning/netting nylon 6 nano-fiber/nets (Fig. 7e) [60]. The sensor changes its color from yellow to red after formaldehyde exposure. the sensor achieved detection limit as low as 50 ppb by naked eyes. Gong et al. exhibited graphene oxide-based colorimetric gas sensor by dip-coating method [65]. While the sensor showed fairly large response to humidity change, it shows better response to ethanol as compared to methanol and NH_3. Another similar work by Chi et al. demonstrated a colorimetric NO_2 sensor using spin-coated graphene oxide and polystyrene sulfonate. The sensor showed visible optical spectrum shifts with fast absorption/desorption time of 200 ms. The detection limit of the sensor was down to 1 ppm at room temperature [66]. A colorimetric NO_2 sensor based on a porous glass impregnated with Saltzman's reagent was reported by Izumi et al [64]. The sensor showed discernable color change, although slow response (30 to 120 min), after NO_2 exposure. A report by Devi et al. showed In_2O_3 commonly used for the micro heater-based gas sensors can also be used for

colorimetric H_2S sensor [66]. Upon exposure to NH_3, the color of In_2O_3 nanostructure was changed due to sulfurization and formation of In_2S_3 layer on the In_2O_3 surface. The sensor exhibited a limit of detection of 10 ppm for H_2S. Kim et al. reported a colorimetric sensor based on a composite nanofiber yarn that is chemically functionalized with an ionic liquid and lead acetate as a colorimetric dye via yarn-spinning technique for H_2S detection. The sensor was able to detect H_2S down to 1 ppm [62]. Owyeung et al. reported washable gas sensing threads for NH_3 detection [63]. The sensor used the dyes 5,10,15,20-Tetraphenyl-21H, 23H-porphine manganese (III) chloride (MnTPP), methyl red (MR), and bromothymol blue (BTB). The gas sensing threads were coated with PDMS which is known to be gas permeable, and the coating keeps dyes on the threads from being washed away in aqueous conditions. It used a smartphone to extract the color changes in red, green, and blue. The sensor was able to detect NH_3 vapor of 10-1000 ppm and HCl. The gas sensors based on plasmonic nanostructures are another type of colorimetric sensors. The refractive index change by the gas absorption of the surrounding medium triggers the spectral change, i.e., interference pattern from the sensor. Especially, H_2 sensor based on plasmonic Pd/Au nanostructures are actively studied in the area, due to the fast change of Pd into PdH_x after H_2 exposures and ability to form an alloy to Au, which is one of the common materials for plasmonic applications due to the wide range of the plasmonic resonance wavelength shift for the diameter changes of the Au nanoparticles. F. Nugroho et al. demonstrated $Pd_{70}Au_{30}$ plasmonic nanodisk structures coated with PTFE/PMMA. The PTFE coating reduced the response time less than 1 s due to the reduction of the activation energies for both H_2 absorption and desorption [67]. The PMMA coating improves H_2 selectivity over interfering cases such as CO_2 and NO_2. Sterl et al. demonstrated plasmonic gas sensor that consists of plasmonic Pd nanoantennas suspended above an Au mirror [68]. The detection mechanism is based on the change of reflected spectrum due to a shift of the plasmonic

resonance. By investigating the geometries of the nanostructure, the optimized sensor demonstrated a detectable signal at 100 ppm H_2. The colorimetric gas sensor consumes no power if the color change can be detected by human eyes. However, more accurate measurement of target gas concentration requires an external light source as well as a detector that consume powers in addition to the well-controlled ambient light conditions. The colorimetric sensor system is composed of the light source, detector, and the sensor. Peter et al. demonstrated colorimetric sensor system that is composed of LED, colorimetric sensing material-coated waveguide, and detector on a single PCB board [69] (Fig. 7f).

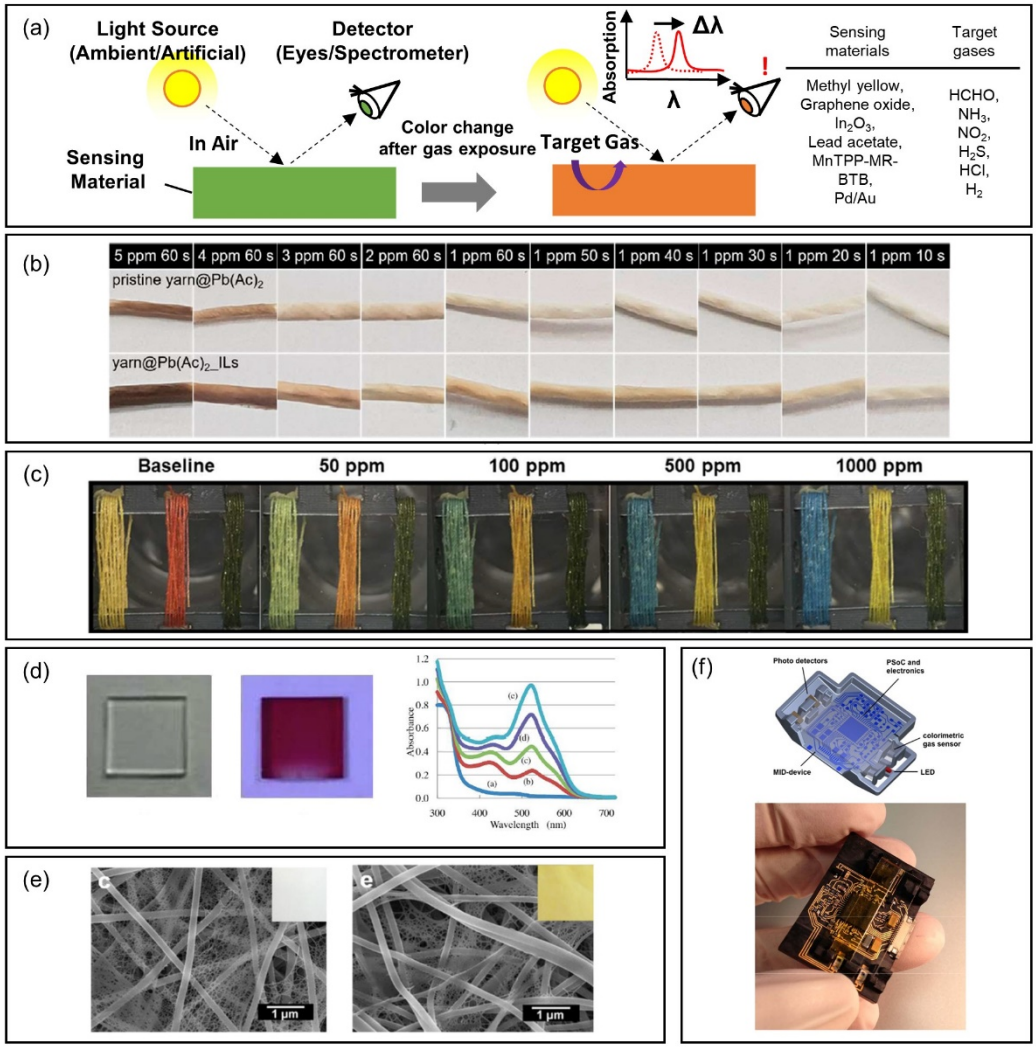

Fig. 7. Various colorimetric gas sensors: (a) Illustrations of colorimetric gas sensors. (b) Changing colors of colorimetric gas sensors based on nanofiber yarn coated with lead acetate (top row) and ionic liquid (bottom row) after exposures to various H_2S concentrations (Reprinted with permission from [62]). (c) Optical images of BTB, MR, and MnTPP devices for different concentrations of NH_3 (Reprinted with permission from [63]). (d) Photographs before and after exposure to NO_2 and spectral changes of NO_2 sensing chips following the exposure of NO_2 for 0, 60, 90, and 120 min (Reprinted with permission from [64]). (e) Reflectance spectra (left) and optical colorimetric response (right) of the Methyl Yellow-

impregnated nylon 6 NFN sensor strips after the exposure to various formaldehyde concentrations (Reprinted with permission from [60]). (f) Sketch (top) and photograph (bottom) of the colorimetric gas sensor module (Reprinted with permission from [69]).

4. Self-powered sensors

4.1. Photovoltaic type

Photovoltaic gas sensors harness ambient light sources such as sunlight and artificial lighting. There are two types of photovoltaic gas sensors. In one type, the gas sensing region is a part of the photovoltaic cell so that the absorption of gas directly modulates the power generation (Fig. 8a). Another type is a photovoltaic gas sensor that has electrically isolated between the gas sensing portion and the photovoltaic cell (Fig. 8b). The gas sensing part is colorimetric sensor that can modulate the spectrum of irradiated light. Because the sensing materials are required to absorb ambient light, most of the photovoltaic sensor has lower energy bandgap ranging in 1.2 – 3 eV. Recently, two-dimensional (2D) material-based photovoltaic sensors are actively researched due to their abilities to absorb ambient light and high sensitivities to the surface state changes upon gas absorption. Lee et al. demonstrated self-powered photovoltaic heterojunctions consisting of a graphene layer in contact with bulk silicon and metal dichalcogenides (Fig. 8c) [8]. The absorbed gas molecules are detected by the chemically-tunable built-in potential of the graphene without electric power consumption. The sensor was able to detect H_2 down to 1 ppm. Niu et al. reported photovoltaic MoS_2/GaSe heterojunction for NO_2 gas sensing (Fig. 8d). The heterojunction was prepared by mechanical exfoliation and dry transfer method. Under 405 nm illumination, the sensor was able to detect NO_2 gas down to 20 ppb [9]. Generally, the base-line signals of photovoltaic gas sensors are largely influenced

by the ambient light conditions. To eliminate the signal drift due to the varying light conditions, a reference photovoltaic device that do not respond to the target gases were used to compensate the signal drift. Kim et al. demonstrated Pd-decorated n-IGZO/p-Si covered with zeolite imidazolate framework-8 (ZIF-8) for H_2 detection [70]. The sensor also used the same structure without Pd decoration to calibrate the base current (Fig. 8e). By using different H_2, O_2 and N_2 gas permeation of ZIF-8, the H_2 sensitivity was greatly improved. Under white light irradiation at zero bias, the sensor showed R_{gas}/R_{air} of 1.57×10^4 % at 1% H_2, response/recovery time < 15 s, and a limit of detection of 35 ppm. Kang et al. reported self-powered gas sensors based on a colorimetric film and organic photovoltaic cell. The colorimetric film was made with Polydimethylsiloxane (PDMS) micro columns and ZnO nanowires hierarchical structures coated with N,N,N',N'-tetramethyl-p-phenylenediamine (TMPD) [71]. The transmittance of TMPD film was reduced upon NO_2 absorption and the current across the photovoltaic cell was reduced accordingly. The response was relatively low with 0.2 ($\Delta I/I_0$) to 20 ppm NO_2, however, it showed good NO_2 selectivity to H_2S and CO. In their sensor configuration, a reference organic photovoltaic cell was used to compensate the base signal drift of the photovoltaic gas sensor (Fig. 8f). Seo et al. demonstrated a H_2 sensor with a Pd film that was asymmetrically coated on a periodic polyurethane acrylate (PUA) nanograting [72]. After the H_2 exposure, the Pd film swells and changes the amount of transmitted light, causing the change of the current output of the photovoltaic cell. Zhao et al. demonstrated photovoltaic gas sensor based on N-hyperdoped microstructured silicon (N-Si). The microstructure on N-Si formed by femtosecond laser creates more defect sites allowing effective gas absorption [73]. An asymmetric illumination on the N-Si forms photo current at zero bias. They tested the NO_2 sensing response with three different wavelengths (455, 730 and 940 nm) and found out that 940 nm illumination shows the best sensing performance overall in terms of the power

consumption, sensitivity, and response time (Fig. 8g).

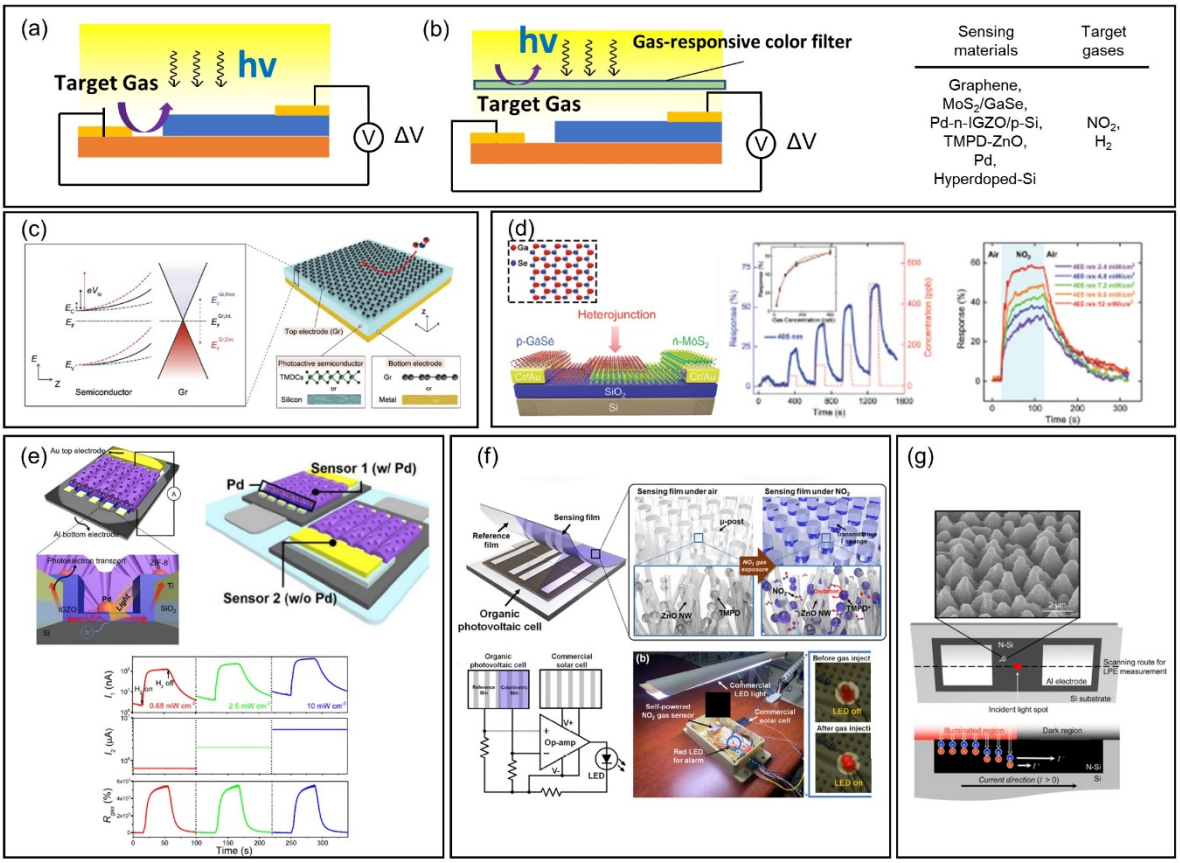

Fig. 8. Schematic illustration of photovoltaic gas sensor structures with (a) direct gas interaction and (b) gas responsive color filter. (c) energy band diagram and schematic illustration of heterojunction photovoltaic gas sensor based on graphene in contact with bulk silicon and metal dichalcogenides (Reprinted with permission from [70]). (d) Schematic illustration and NO_2 sensing characteristics of photovoltaic MoS_2/GaSe gas sensor (Reprinted with permission from [9]). (e) Schematic illustration of Pd-decorated n-IGZO/p-Si covered with zeolite imidazolate framework-8 (ZIF-8). A reference n-IGZO/p-Si structure was used for the signal drift correction (Reprinted with permission from [70]). (f) Schematic illustration, circuit diagram and photograph of colorimetric film-based photovoltaic gas sensor using hierarchical micro/nano-structures coated with TMPD for NO_2 detection (Reprinted with

permission from [71]). (g) SEM image of N-hyperdoped microstructured silicon surface and schematic illustration of current generation in the structure using asymmetric illumination (Reprinted with permission from [73]).

4.2. Triboelectric type

Triboelectric uses electrostatic phenomena that is most common in nature. Dipole charges are created by a mechanical friction at the contacting surface, and the electrostatic induction generates voltage potential/current across an external load [74]. The current generated across the external load by triboelectric is described as:

$$I = \mathrm{C}\frac{\partial \mathrm{V}}{\partial \mathrm{t}} + \mathrm{V}\frac{\partial \mathrm{C}}{\partial \mathrm{t}}$$

where C is capacitance and V is voltage potential.

Triboelectric gas sensor uses the changes of open-circuit voltage or short-circuit current upon absorption/desorption of the target gas at the contacting surface (Fig. 9a). Uddin et al. demonstrated a triboelectric H_2 sensor based on micro-pyramid PDMS film and Pd nanoparticle-decorated ZnO nanorods array (Fig. 9b) [75]. When the sensor was exposed to H_2, the chemisorbed oxygen ions ($O^-_{2(ads)}$) forms H_2O releasing free electrons, and the free electrons effectively screen the triboelectric effect. The senor showed maximum response of 373 %, response time of 100 s to 10,000 ppm H_2 and limit of detection of 10 ppm. Cai et al. showed porous wood-based triboelectric gas sensors for the NH_3 detection (Fig. 9c) [76]. The fabrication of porous wood starts from the removal of lignin/hemicellulose from a natural wood followed by soaking in CNT solution. The CNT-treated conductive wood exhibits better

mechanical rigidity as compared to the untreated one. The working principle of the conductive wood based triboelectric gas sensor is similar to the work of Uddin et al. $O^-_{2(ads)}$ forms on the wood surface and reacts to NH_3, and the reaction creates free electrons reducing the resistance of the wood. The conductive wood-based triboelectric gas sensor was able to detect NH_3 gas from 50 – 500 ppm maintaining good stability under high humidity (75%) and low temperature (-18 ^oC) conditions. Cui et al. exhibited conducting polyaniline (PANI) nanofiber-based triboelectric NH_3 sensor [7]. The sensor mechanism is based on the conversion of non-conductive emeraldine base polyaniline (N-PANI) to conductive emeraldine salt polyaniline (C-PANI) by deprotonation upon exposure to NH_3. The resistivity of the PANI and output voltage are reduced upon NH_3 exposure. The sensor can detect NH_3 ranging in 500 – 10000 ppm. Several papers reported triboelectric generators as the power source to operate gas sensors. Zhao et al. developed self-powered CO_2 sensor based on gas discharge [77]. Varying the distance between tip-plate electrodes and negative/positive discharge method, the sensor could detect NH_3 with different concentrations ranging in 1000 – 200000 ppm (Fig. 9d). Hong et al. demonstrated a triboelectric NO_2 sensor based on corrugated PDMS and 3D-graphene/CNT [78]. The sensor was able to detect 1 ppm NO_2 with maximum response of 66.1 %. The limit of detection of the sensor was 10 ppb. Gu et al. showed light-enhanced WS_2 microflake gas sensor with an LED powered by a triboelectric nanogenerator [10]. The sensor shows selectivity to 10 pm NH_3 as compared to several gases such as formaldehyde, methanol, acetone, benzene, ethanol and methylbenzene (60 ppm each). Triboelectric gas sensors have advantages of operating the gas sensor without external power sources. However, the triboelectric generators are required to provide consistent baseline signals provided by mechanical friction. Furthermore, like other types of room-temperature gas sensors, humidity largely affects the sensor signal. These issues must be solved for triboelectric gas sensors for

more accurate and reliable gas sensing.

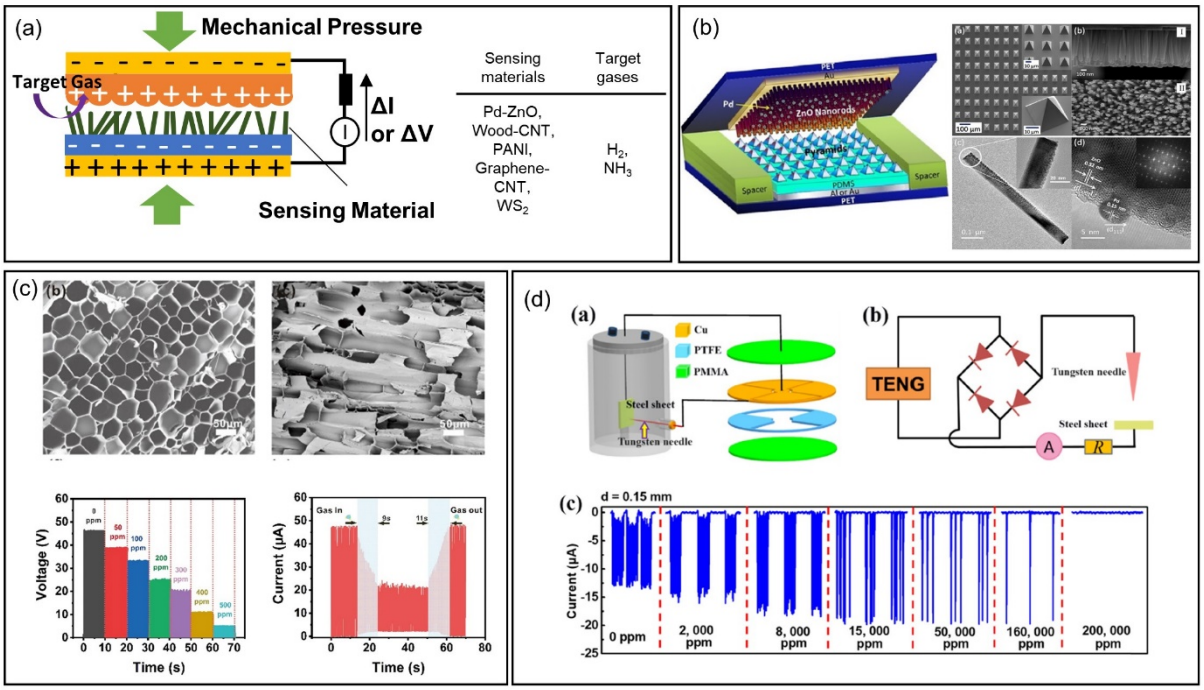

Fig. 9. (a) Schematic illustration of general triboelectric gas sensors. (b) Schematic illustration, SEM and TEM images of the triboelectric gas sensor using Pd nanoparticle-decorated micro-pyramid PDMS film structure (Reprinted with permission from [75]). (c) SEM image and sensing responses of CNT-treated porous wood-based triboelectric gas sensor after exposures to various NH_3 concentrations (Reprinted with permission from [76]). (d) Schematic illustration and CO_2 sensing responses of self-powered gas discharge base gas sensor (Reprinted with permission from [77]).

4.3. Piezoelectric type

Similar to the triboelectricity, piezoelectric signal of materials can be a function of gas concentration and simultaneously harvest energy (Fig. 10a). The free charge carrier density in

a material is changed by the surface charge density following the gas adsorption. This causes a piezoelectric screening effect and thus change the piezoelectric output [79]. Nanowires have been used for piezoelectric gas sensors because of its high SVR.

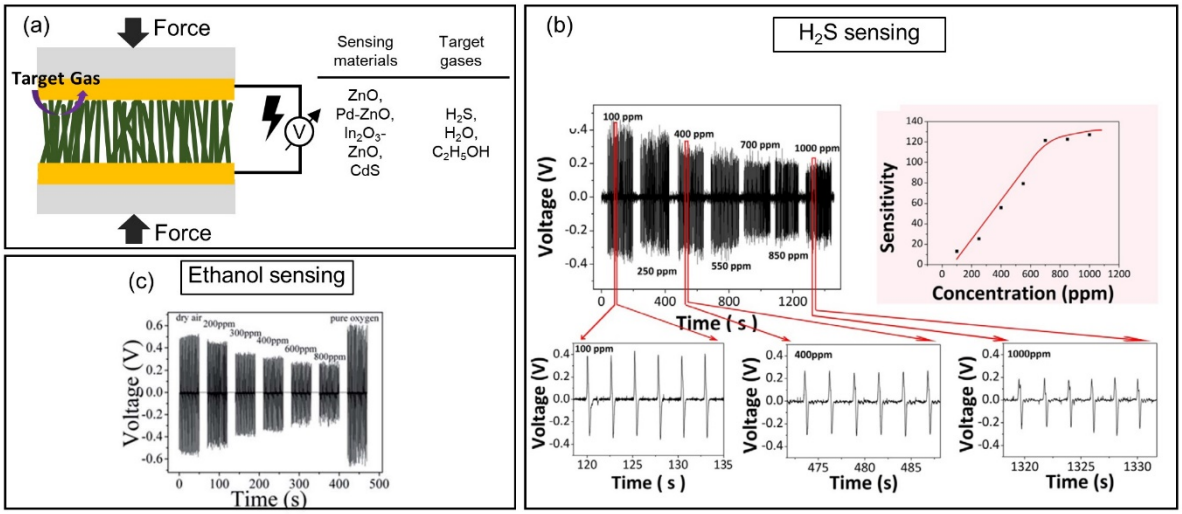

Fig. 10. Various piezoelectric gas sensors: (a) Schematic of piezoelectric gas sensor, (b) H_2S response of ZnO nanowire (Reprinted with permission from [79]), (c) Ethanol response of Pd-ZnO nanowire under repeated compression (Reprinted with permission from [80]).

Xue et al. developed a piezoelectric type gas sensor using ZnO nanowire arrays (Fig. 10b) [79]. The piezoelectric response of ZnO is affected by the surrounding gases (e.g. H_2S). ZnO nanowire array was grown on a titanium substrate using a hydrothermal method and covered by a flexible aluminum foil. Piezoelectric responses with dry air, oxygen, H_2S and high relative humidity were characterized. Because oxygen widened the depletion layer of ZnO nanowire, the piezoelectric response in oxygen atmosphere increased as compared to dry air. On the other hand, the piezoelectric responses in H_2S and water vapor atmosphere decreased because of narrow depletion layer. The H_2S concentration dependence of response was characterized and

showed a linear relationship up to 700 ppm. Lin et al. from the same research group demonstrated a Pd coated ZnO nanowire array for ethanol gas sensor (Fig. 10c) [80]. Adsorbed oxygens produced by the spillover effect on Pd nanoparticles covered the surface of the ZnO nanowires and were partially removed by reacting with ethanol gas. This removal decreased the depletion layer of ZnO nanowire, resulting in a lower piezoelectric response. Their group reported a core-shell structure of In_2O_3/ZnO and cadmium sulfide nanorod arrays for H_2S gas sensors [81]. A ZnO nanowire array was prepared by a hydrothermal method and In_2O_3 was coated on the ZnO nanowires by immersing an indium nitrate solution. By the heterostructure, piezoelectric response to 700 ppm of H_2S gas was enhanced by 7 times compared to bare ZnO nanowires. Cadmium sulfide nanorods grown on titanium foil using a hydrothermal method and H_2S gas sensing behavior was characterized [82]. Similar to the triboelectric gas sensors, piezoelectric gas sensor can detect the gases without external power sources. However, because piezoelectric signal depends on not only the gas concentration but also the strain and strain rate, the sensor needs to be integrated with a mechanical system that can produce consistent strain rate. In fact, the mechanical system requires external electrical power. In addition, the choice of materials is limited because the sensing materials are highly crystalline and nanowire structure.

5. Conclusion

This paper reviewed various nanostructure-based gas sensors based on the power consumption and sensing mechanism points of view. mechanism points of view. The sensors were categorized according to the power consumption. Microheater platform-based chemiresistive, calorimetric, electrochemical and self-heated multi-nanowire-based type gas

sensors were classified into the low power group with a power consumption from 1 to 100 mW. Self-heated single-nanowire-based, photo-activated, capacitive, and colorimetric type gas sensors were classified into the ultralow power group with a power consumption less than 1 mW down to zero. Photovoltaic, triboelectric, and piezoelectric gas sensors were classified into the self-power group with power generation during sensor operation.

The adoption of low dimensional materials such as nanowires or 2D materials helped to achieve gas sensing with low power consumption. Since the microheater based gas sensors have been developed for two decades, low power gas sensors are commercially available in the market. Novel microheater designs and sensing material coating methods have enabled to lower the power consumption of gas sensors. The power consumption of microheaters has been lowered by reducing heat dissipation with innovative structures, such as suspended membrane, bridged microplate, bridge, and beam. Power consumption can be further lowered by narrowing the size of bridge and utilizing low thermal conductive materials. Advanced manufacturing methods for microheaters need to be developed in order to fabricate mechanically robust structure in microscale. In addition, coating methods for integrating sensing materials on the small microheater platforms and gas sensing materials with low working temperature have to be developed. Nanostructure-based sensing materials not only enhance the sensing performance but also allow them to be deposited on various MEMS platforms via various printing techniques.

Power consumption of self-heated nanowire gas sensors depends on the number of heated nanowires. Fewer nanowires or single nanowire can lower the power consumption down to few tens of microwatt. However, because of the fabrication complexity and limited material selection, single nanowire based self-heated gas sensors have not been explored in depth.

Advanced contact transfer printing or inkjet printing of pre-grown nanowire could make it easy to fabricate the sensors. The photo-activated gas sensors use light sources that can excite electron-hole pairs and they involve with the gas adsorption/desorption. Using nanostructures with appropriate bandgap to help light absorption improves the sensitivity by generating more electron/hole pairs which involves the gas absorption/desorption process, and also plasmonic or catalytic nanoparticle coatings enhances light absorption and gas sensitivity. The use of low-power light source such as micro-LED can help to reduce the overall power consumption of the sensors drastically. Colorimetric gas sensors do not consume any power. However, in reality, many colorimetric gas sensors require controlled light condition and spectrometer. Integrating the colorimetric sensor system is required to reduce the overall power consumption of colorimetric gas sensors. Capacitive sensors using nanostructured film are very sensitive to target gases, but they are very susceptible to high humidity. Adopting micro/nano heaters would be a solution in expense of increasing power consumption.

Self-powered gas sensors have some hurdles to overcome for practical applications. Since these sensor works at room temperature, slow response time and susceptibility to external disturbances are the biggest problems. Signal processing using machine learning technique with temperature/humidity sensors could improve the gas sensing performance. For piezoelectric gas sensors, the screening effect of nanowires makes different piezoelectric voltages under gas environment. The sensing response of self-powered gas sensor depends on not only gases but also power sources, such as photon energy or mechanical energy. To compensate for the disturbance of these power sources, self-powered sensors with a reference sensor have been developed. However, there are still power supply issues such as limited power source for photovoltaic sensors at night, and consistent mechanical stimulation for triboelectric

and piezoelectric gas sensors. Integrating other types of gas sensors with self-powered gas sensors could be the one of the solutions to resolve this.

Declaration of Competing Interest

The authors declare no conflict of interest.

Acknowledgments

This work was supported by the National Research Foundation of Korea (NRF) grant funded by the Korea government (MSIT) (No. 2021R1A2C3008742).

References

[1] Y. Development, Gas and Particle Sensors - Technology and Market Trends 2021 report, 2021.

[2] J. Seo, Y. Lim, H. Shin, Self-heating hydrogen gas sensor based on an array of single suspended carbon nanowires functionalized with palladium nanoparticles, Sensors and Actuators B: Chemical, 247 (2017) 564-72. https://doi.org/10.1016/j.snb.2017.03.038.

[3] J. Yun, J. Ahn, Y. Choi, I. Park, Ultra-low power hydrogen sensor by suspended and palladium coated silicon nanowire, 2017 IEEE 30th International Conference on Micro Electro Mechanical Systems (MEMS)2017, pp. 1079-82.

[4] J. Zhang, E. Strelcov, A. Kolmakov, Heat dissipation from suspended self-heated nanowires: gas sensor prospective, Nanotechnology, 24 (2013) 444009. https://doi.org/10.1088/0957-4484/24/44/444009.

[5] S. Park, S. An, Y. Mun, C. Lee, UV-Enhanced NO2 Gas Sensing Properties of SnO2-Core/ZnO-Shell Nanowires at Room Temperature, ACS Applied Materials & Interfaces, 5 (2013) 4285-92. https://doi.org/10.1021/am400500a.

[6] Y.-M. Jo, K. Lim, J.W. Yoon, Y.K. Jo, Y.K. Moon, H.W. Jang, et al., Visible-Light-Activated Type II Heterojunction in Cu3(hexahydroxytriphenylene)2/Fe2O3 Hybrids for Reversible NO2 Sensing: Critical Role of π–π* Transition, ACS Central Science, 7 (2021) 1176-82. https://doi.org/10.1021/acscentsci.1c00289.

[7] S. Cui, Y. Zheng, T. Zhang, D. Wang, F. Zhou, W. Liu, Self-powered ammonia nanosensor based on the integration of the gas sensor and triboelectric nanogenerator, Nano Energy, 49 (2018) 31-9. https://doi.org/10.1016/j.nanoen.2018.04.033.

[8] D. Lee, H. Park, S.D. Han, S.H. Kim, W. Huh, J.Y. Lee, et al., Self-Powered Chemical Sensing Driven by Graphene-Based Photovoltaic Heterojunctions with Chemically Tunable Built-In Potentials, Small, 15 (2019) 1804303. https://doi.org/10.1002/smll.201804303.

[9] Y. Niu, J. Zeng, X. Liu, J. Li, Q. Wang, H. Li, et al., A Photovoltaic Self-Powered Gas Sensor Based on All-Dry Transferred MoS2/GaSe Heterojunction for ppb-Level NO2 Sensing at Room Temperature, Advanced Science, 8 (2021) 2100472. https://doi.org/10.1002/advs.202100472.

[10] D. Gu, X. Li, H. Wang, M. Li, Y. Xi, Y. Chen, et al., Light enhanced VOCs sensing of WS2 microflakes based chemiresistive sensors powered by triboelectronic nangenerators, Sensors and Actuators B: Chemical, 256 (2018) 992-1000. https://doi.org/10.1016/j.snb.2017.10.045.

[11] J. Courbat, D. Briand, L. Yue, S. Raible, N. De Rooij, Drop-coated metal-oxide gas sensor on polyimide foil with reduced power consumption for wireless applications, Sensors and Actuators B: Chemical, 161 (2012) 862-8. https://doi.org/10.1016/j.snb.2011.11.050.

[12] M. Kim, H. Mi, M. Cho, J.H. Seo, W. Zhou, S. Gong, et al., Appl Phys Lett, 106 (2015) 212107.

[13] X. Wang, P. Xu, L. Tang, Y. Chen, X. Li, Nano beta zeolites catalytic-cracking effect on hydrochlorofluorocarbon molecule for specific detection of Freon, Journal of Materials Chemistry A, 9 (2021) 15321-8. https://doi.org/10.1039/D1TA02928B.

[14] S. Moon, H.-K. Lee, N. Choi, H. Kang, J. Lee, S. Ahn, et al., Low power consumption micro C2H5OH gas sensor based on micro-heater and ink jetting technique, Sensors and Actuators B: Chemical, 217 (2015) 146-50. https://doi.org/10.1016/j.snb.2014.10.034.

[15] K. Kang, D. Yang, J. Park, S. Kim, I. Cho, H.-H. Yang, et al., Micropatterning of metal oxide nanofibers by electrohydrodynamic (EHD) printing towards highly integrated and multiplexed gas sensor applications, Sensors and Actuators B: Chemical, 250 (2017) 574-83. https://doi.org/10.1016/j.snb.2017.04.194.

[16] Z. Dai, L. Xu, G. Duan, T. Li, H. Zhang, Y. Li, et al., Fast-response, sensitivitive and low-powered chemosensors by fusing nanostructured porous thin film and IDEs-microheater chip, Sci Rep, 3 (2013) 1669. https://doi.org/10.1038/srep01669.

[17] H. Long, A. Harley-Trochimczyk, T. He, T. Pham, Z. Tang, T. Shi, et al., In situ localized growth of porous tin oxide films on low power microheater platform for low temperature CO detection, Acs Sensors, 1 (2016) 339-43. https://doi.org/10.1021/acssensors.5b00302.

[18] A. Rao, H. Long, A. Harley-Trochimczyk, T. Pham, A. Zettl, C. Carraro, et al., In Situ Localized Growth of Ordered Metal Oxide Hollow Sphere Array on Microheater Platform for Sensitive, Ultra-Fast Gas Sensing, ACS Appl Mater Interfaces, 9 (2017) 2634-41. https://doi.org/10.1021/acsami.6b12677.

[19] I. Cho, K. Kang, D. Yang, J. Yun, I. Park, Localized Liquid-Phase Synthesis of Porous SnO2 Nanotubes on MEMS Platform for Low-Power, High Performance Gas Sensors, ACS

Appl Mater Interfaces, 9 (2017) 27111-9. https://doi.org/10.1021/acsami.7b04850.

[20] D. Xu, P. Xu, X. Wang, Y. Chen, H. Yu, D. Zheng, et al., Pentagram-Shaped Ag@ Pt Core–Shell Nanostructures as High-Performance Catalysts for Formaldehyde Detection, ACS Applied Materials & Interfaces, 12 (2020) 8091-7. https://doi.org/10.1021/acsami.9b17201.

[21] K.-W. Choi, J.-S. Lee, M.-H. Seo, M.-S. Jo, J.-Y. Yoo, G.S. Sim, et al., Batch-fabricated CO gas sensor in large-area (8-inch) with sub-10 mW power operation, Sensors and Actuators B: Chemical, 289 (2019) 153-9. https://doi.org/10.1016/j.snb.2019.03.074.

[22] K.W. Choi, M.S. Jo, J.S. Lee, J.Y. Yoo, J.B. Yoon, Perfectly Aligned, Air-Suspended Nanowire Array Heater and Its Application in an Always-On Gas Sensor, Adv Funct Mater, 30 (2020) 2004448. https://doi.org/10.1002/adfm.202004448.

[23] L.F. Zhu, J.C. She, J.Y. Luo, S.Z. Deng, J. Chen, X.W. Ji, et al., Self-heated hydrogen gas sensors based on Pt-coated W18O49 nanowire networks with high sensitivity, good selectivity and low power consumption, Sensors and Actuators B: Chemical, 153 (2011) 354-60. https://doi.org/10.1016/j.snb.2010.10.047.

[24] H.M. Tan, C. Manh Hung, T.M. Ngoc, H. Nguyen, N. Duc Hoa, N. Van Duy, et al., Novel self-heated gas sensors using on-chip networked nanowires with ultralow power consumption, ACS applied materials & interfaces, 9 (2017) 6153-62. https://doi.org/10.1021/acsami.6b14516.

[25] T.M. Ngoc, N. Van Duy, C.M. Hung, N.D. Hoa, N.N. Trung, H. Nguyen, et al., Ultralow power consumption gas sensor based on a self-heated nanojunction of SnO 2 nanowires, RSC advances, 8 (2018) 36323-30. https://doi.org/10.1039/C8RA06061D.

[26] J.-H. Kim, A. Mirzaei, H.W. Kim, S.S. Kim, Low-voltage-driven sensors based on ZnO nanowires for room-temperature detection of NO2 and CO gases, ACS applied materials & interfaces, 11 (2019) 24172-83. https://doi.org/10.1021/acsami.9b07208.

[27] J.S. Lee, K.W. Choi, J.Y. Yoo, M.S. Jo, J.B. Yoon, Realization of Nanolene: A Planar Array of Perfectly Aligned, Air-Suspended Nanowires, Small, 16 (2020) 1906845. https://doi.org/10.1002/smll.201906845.

[28] E.-B. Lee, I.-S. Hwang, J.-H. Cha, H.-J. Lee, W.-B. Lee, J.J. Pak, et al., Micromachined catalytic combustible hydrogen gas sensor, Sensors and Actuators B: Chemical, 153 (2011) 392-7. https://doi.org/10.1016/j.snb.2010.11.004.

[29] A.S. Pranti, D. Loof, S. Kunz, V. Zielasek, M. Bäumer, W. Lang, Highly sensitive and selective hydrogen gas sensor with platinum nanoparticles linked by 4, 4"-diamino-P-terphenyl (dater), 2019 20th International Conference on Solid-State Sensors, Actuators and Microsystems & Eurosensors XXXIII (TRANSDUCERS & EUROSENSORS XXXIII), IEEE2019, pp. 326-9.

[30] A. Harley-Trochimczyk, J. Chang, Q. Zhou, J. Dong, T. Pham, M.A. Worsley, et al., Catalytic hydrogen sensing using microheated platinum nanoparticle-loaded graphene aerogel, Sensors and Actuators B: Chemical, 206 (2015) 399-406. https://doi.org/10.1016/j.snb.2014.09.057.

[31] D.V. Del Orbe, H. Yang, I. Cho, J. Park, J. Choi, S.W. Han, et al., Low-power thermocatalytic hydrogen sensor based on electrodeposited cauliflower-like nanostructured Pt black, Sensors and Actuators B: Chemical, 329 (2021) 129129. https://doi.org/10.1016/j.snb.2020.129129.

[32] L. Li, S. Niu, Y. Qu, Q. Zhang, H. Li, Y. Li, et al., One-pot synthesis of uniform mesoporous rhodium oxide/alumina hybrid as high sensitivity and low power consumption methane catalytic combustion micro-sensor, J Mater Chem, 22 (2012) 9263-7. https://doi.org/10.1039/C2JM15870A.

[33] E. Brauns, E. Morsbach, G. Schnurpfeil, M. Bäumer, W. Lang, A miniaturized catalytic

gas sensor for hydrogen detection based on stabilized nanoparticles as catalytic layer, Sensors and Actuators B: Chemical, 187 (2013) 420-5. https://doi.org/10.1016/j.snb.2013.01.037.

[34] E. Brauns, E. Morsbach, S. Kunz, M. Bäumer, W. Lang, A fast and sensitive catalytic gas sensors for hydrogen detection based on stabilized nanoparticles as catalytic layer, Sensors and Actuators B: Chemical, 193 (2014) 895-903. https://doi.org/10.1016/j.snb.2013.11.048.

[35] A. Harley-Trochimczyk, A. Rao, H. Long, A. Zettl, C. Carraro, R. Maboudian, Low-power catalytic gas sensing using highly stable silicon carbide microheaters, Journal of Micromechanics and Microengineering, 27 (2017) 045003. https://doi.org/10.1088/1361-6439/aa5d70.

[36] E.E. Karpov, E.F. Karpov, A. Suchkov, S. Mironov, A. Baranov, V. Sleptsov, et al., Energy efficient planar catalytic sensor for methane measurement, Sensors and Actuators A: Physical, 194 (2013) 176-80. https://doi.org/10.1016/j.sna.2013.01.057.

[37] D. Del Orbe Henriquez, I. Cho, H. Yang, J. Choi, M. Kang, K.S. Chang, et al., Pt Nanostructures Fabricated by Local Hydrothermal Synthesis for Low-Power Catalytic-Combustion Hydrogen Sensors, ACS Applied Nano Materials, 4 (2020) 7-12. https://doi.org/10.1021/acsanm.0c02794.

[38] J. Lee, N. Choi, H. Lee, J. Kim, S. Lim, J. Kwon, et al., Low power consumption solid electrochemical-type micro CO2 gas sensor, Sensors and Actuators B: Chemical, 248 (2017) 957-60. https://doi.org/10.1016/j.snb.2017.02.040.

[39] J. Prades, R. Jimenez-Diaz, F. Hernandez-Ramirez, S. Barth, A. Cirera, A. Romano-Rodriguez, et al., Ultralow power consumption gas sensors based on self-heated individual nanowires, Appl Phys Lett, 93 (2008) 123110. https://doi.org/10.1063/1.2988265.

[40] K. Chikkadi, M. Muoth, V. Maiwald, C. Roman, C. Hierold, Ultra-low power operation of self-heated, suspended carbon nanotube gas sensors, Appl Phys Lett, 103 (2013) 223109.

https://doi.org/10.1063/1.4836415.

[41] J. Yun, C.Y. Jin, J.-H. Ahn, S. Jeon, I. Park, A self-heated silicon nanowire array: selective surface modification with catalytic nanoparticles by nanoscale Joule heating and its gas sensing applications, Nanoscale, 5 (2013) 6851-6. https://doi.org/10.1039/C3NR01640D.

[42] J.-H. Ahn, J. Yun, D.-I. Moon, Y.-K. Choi, I. Park, Self-heated silicon nanowires for high performance hydrogen gas detection, Nanotechnology, 26 (2015) 095501. https://doi.org/10.1088/0957-4484/26/9/095501.

[43] J. Yun, J.-H. Ahn, D.-I. Moon, Y.-K. Choi, I. Park, Joule-heated and suspended silicon nanowire based sensor for low-power and stable hydrogen detection, ACS applied materials & interfaces, 11 (2019) 42349-57. https://doi.org/10.1021/acsami.9b15111.

[44] M. Afshar, E.M. Preiß, T. Sauerwald, M. Rodner, D. Feili, M. Straub, et al., Indium-tin-oxide single-nanowire gas sensor fabricated via laser writing and subsequent etching, Sensors and Actuators B: Chemical, 215 (2015) 525-35. https://doi.org/10.1016/j.snb.2015.03.067.

[45] M. Cho, I. Park, Recent Trends of Light-enhanced Metal Oxide Gas Sensors: Review, Journal of Sensor Science and Technology, 25 (2016) 103-9. https://doi.org/10.5369/JSST.2016.25.2.103.

[46] Y.M. Sabri, A.E. Kandjani, S.S.A.A.H. Rashid, C.J. Harrison, S.J. Ippolito, S.K. Bhargava, Soot template TiO2 fractals as a photoactive gas sensor for acetone detection, Sensors and Actuators B: Chemical, 275 (2018) 215-22. https://doi.org/10.1016/j.snb.2018.08.059.

[47] L. Han, D. Wang, J. Cui, L. Chen, T. Jiang, Y. Lin, Study on formaldehyde gas-sensing of In2O3-sensitized ZnO nanoflowers under visible light irradiation at room temperature, Journal of Materials Chemistry, 22 (2012) 12915-20. https://doi.org/10.1039/C2JM16105B.

[48] I. Cho, Y.C. Sim, M. Cho, Y.-H. Cho, I. Park, Monolithic Micro Light-Emitting Diode/Metal Oxide Nanowire Gas Sensor with Microwatt-Level Power Consumption, ACS

Sensors, 5 (2020) 563-70. https://doi.org/10.1021/acssensors.9b02487.

[49] H.-Y. Li, J.-W. Yoon, C.-S. Lee, K. Lim, J.-W. Yoon, J.-H. Lee, Visible light assisted NO2 sensing at room temperature by CdS nanoflake array, Sensors and Actuators B: Chemical, 255 (2018) 2963-70. https://doi.org/10.1016/j.snb.2017.09.118.

[50] Y.K. Jo, S.-Y. Jeong, Y.K. Moon, Y.-M. Jo, J.-W. Yoon, J.-H. Lee, Exclusive and ultrasensitive detection of formaldehyde at room temperature using a flexible and monolithic chemiresistive sensor, Nature Communications, 12 (2021) 4955. https://doi.org/10.1038/s41467-021-25290-3.

[51] K. Lim, Y.-M. Jo, J.-W. Yoon, J.-S. Kim, D.-J. Lee, Y.K. Moon, et al., A Transparent Nanopatterned Chemiresistor: Visible-Light Plasmonic Sensor for Trace-Level NO2 Detection at Room Temperature, Small, 17 (2021) 2100438. https://doi.org/10.1002/smll.202100438.

[52] S. Zeinali, S. Homayoonnia, G. Homayoonnia, Comparative investigation of interdigitated and parallel-plate capacitive gas sensors based on Cu-BTC nanoparticles for selective detection of polar and apolar VOCs indoors, Sensors and Actuators B: Chemical, 278 (2019) 153-64. https://doi.org/10.1016/j.snb.2018.07.006.

[53] Z. Zhai, X. Zhang, X. Hao, B. Niu, C. Li, Metal–Organic Frameworks Materials for Capacitive Gas Sensors, 6 (2021) 2100127. https://doi.org/10.1002/admt.202100127.

[54] M.A. Andrés, M.T. Vijjapu, S.G. Surya, O. Shekhah, K.N. Salama, C. Serre, et al., Methanol and Humidity Capacitive Sensors Based on Thin Films of MOF Nanoparticles, ACS Applied Materials & Interfaces, 12 (2020) 4155-62. https://doi.org/10.1021/acsami.9b20763.

[55] A.H. Assen, O. Yassine, O. Shekhah, M. Eddaoudi, K.N. Salama, MOFs for the Sensitive Detection of Ammonia: Deployment of fcu-MOF Thin Films as Effective Chemical Capacitive Sensors, ACS Sensors, 2 (2017) 1294-301. https://doi.org/10.1021/acssensors.7b00304.

[56] H. Yamazaki, Y. Hayashi, K. Masunishi, D. Ono, T. Ikehashi, High sensitivity MEMS

capacitive hydrogen sensor with inverted T-shaped electrode and ring-shaped palladium alloy for fast response and low power consumption, Journal of Micromechanics and Microengineering, 28 (2018) 094001. https://doi.org/10.1088/1361-6439/aac21d.

[57] T. Subbiah, G.S. Bhat, R.W. Tock, S. Parameswaran, S.S. Ramkumar, Electrospinning of nanofibers, Journal of Applied Polymer Science, 96 (2005) 557-69. https://doi.org/10.1002/app.21481.

[58] N. Bhardwaj, S.C. Kundu, Electrospinning: A fascinating fiber fabrication technique, Biotechnology Advances, 28 (2010) 325-47. https://doi.org/10.1016/j.biotechadv.2010.01.004.

[59] M.O. Kim, M.Q. Khan, A. Ullah, N.P. Duy, C. Zhu, J.-S. Lee, et al., Development of VOCs gas sensor with high sensitivity using colorimetric polymer nanofiber: a unique sensing method, Materials Research Express, 6 (2019) 105372. https://doi.org/10.1088/2053-1591/ab42a5.

[60] X. Wang, Y. Si, J. Wang, B. Ding, J. Yu, S.S. Al-Deyab, A facile and highly sensitive colorimetric sensor for the detection of formaldehyde based on electro-spinning/netting nano-fiber/nets, Sensors and Actuators B: Chemical, 163 (2012) 186-93. https://doi.org/10.1016/j.snb.2012.01.033.

[61] Y.-Y. Lv, J. Wu, Z.-K. Xu, Colorimetric and fluorescent sensor constructing from the nanofibrous membrane of porphyrinated polyimide for the detection of hydrogen chloride gas, Sensors and Actuators B: Chemical, 148 (2010) 233-9. https://doi.org/10.1016/j.snb.2010.05.029.

[62] D.-H. Kim, J.-H. Cha, J.Y. Lim, J. Bae, W. Lee, K.R. Yoon, et al., Colorimetric Dye-Loaded Nanofiber Yarn: Eye-Readable and Weavable Gas Sensing Platform, ACS Nano, 14 (2020) 16907-18. https://doi.org/10.1021/acsnano.0c05916.

[63] R.E. Owyeung, M.J. Panzer, S.R. Sonkusale, Colorimetric Gas Sensing Washable Threads for Smart Textiles, Scientific Reports, 9 (2019) 5607. https://doi.org/10.1038/s41598-019-

42054-8.

[64] K. Izumi, M. Utiyama, Y.Y. Maruo, Colorimetric NOx sensor based on a porous glass-based NO2 sensing chip and a permanganate oxidizer, Sensors and Actuators B: Chemical, 216 (2015) 128-33. https://doi.org/10.1016/j.snb.2015.04.029.

[65] T. Gong, X. Zhang, Y. Fu, G. Zhou, H. Chi, T. Li, A facile fabrication of colorimetric graphene oxide reflecting films for ultrasensitive optical gas sensing, Sensors and Actuators B: Chemical, 261 (2018) 83-90. https://doi.org/10.1016/j.snb.2018.01.137.

[66] H. Chi, Z. Xu, X. Duan, J. Yang, F. Wang, Z. Li, High-Performance Colorimetric Room-Temperature NO2 Sensing Using Spin-Coated Graphene/Polyelectrolyte Reflecting Film, ACS Applied Materials & Interfaces, 11 (2019) 32390-7. https://doi.org/10.1021/acsami.9b09901.

[67] F.A.A. Nugroho, I. Darmadi, L. Cusinato, A. Susarrey-Arce, H. Schreuders, L.J. Bannenberg, et al., Metal–polymer hybrid nanomaterials for plasmonic ultrafast hydrogen detection, Nature Materials, 18 (2019) 489-95. https://doi.org/10.1038/s41563-019-0325-4.

[68] F. Sterl, N. Strohfeldt, S. Both, E. Herkert, T. Weiss, H. Giessen, Design Principles for Sensitivity Optimization in Plasmonic Hydrogen Sensors, ACS Sensors, 5 (2020) 917-27. https://doi.org/10.1021/acssensors.9b02436.

[69] C. Peter, S. Schulz, M. Barth, M. Gempp, S. Rademacher, J. Wöllenstein, Low-cost roll-to-roll colorimetric gas sensor system for fire detection, 2013 Transducers & Eurosensors XXVII: The 17th International Conference on Solid-State Sensors, Actuators and Microsystems (TRANSDUCERS & EUROSENSORS XXVII)2013, pp. 2632-5.

[70] H. Kim, W. Kim, R. Lee, S. Cho, J. Park, Y. Pak, et al., High-Performance Photovoltaic Hydrogen Sensing Platform with a Light-Intensity Calibration Module, ACS Sensors, 5 (2020) 1050-7. https://doi.org/10.1021/acssensors.9b02565.

[71] K. Kang, J. Park, B. Kim, K. Na, I. Cho, J. Rho, et al., Self-Powered Gas Sensor Based on

a Photovoltaic Cell and a Colorimetric Film with Hierarchical Micro/Nanostructures, ACS Applied Materials & Interfaces, 12 (2020) 39024-32. https://doi.org/10.1021/acsami.0c08128.

[72] M.-H. Seo, K. Kang, J.-Y. Yoo, J. Park, J.-S. Lee, I. Cho, et al., Chemo-Mechanically Operating Palladium-Polymer Nanograting Film for a Self-Powered H2 Gas Sensor, ACS Nano, 14 (2020) 16813-22. https://doi.org/10.1021/acsnano.0c05476.

[73] Y. Zhao, X.-L. Liu, S.-X. Ma, W.-J. Wang, X.-J. Ning, L. Zhao, et al., Light-optimized photovoltaic self-powered NO2 gas sensing based on black silicon, Sensors and Actuators B: Chemical, 340 (2021) 129985. https://doi.org/10.1016/j.snb.2021.129985.

[74] F.-R. Fan, Z.-Q. Tian, Z. Lin Wang, Flexible triboelectric generator, Nano Energy, 1 (2012) 328-34. https://doi.org/10.1016/j.nanoen.2012.01.004.

[75] A.S.M.I. Uddin, G.-S. Chung, A self-powered active hydrogen gas sensor with fast response at room temperature based on triboelectric effect, Sensors and Actuators B: Chemical, 231 (2016) 601-8. https://doi.org/10.1016/j.snb.2016.03.063.

[76] C. Cai, J. Mo, Y. Lu, N. Zhang, Z. Wu, S. Wang, et al., Integration of a porous wood-based triboelectric nanogenerator and gas sensor for real-time wireless food-quality assessment, Nano Energy, 83 (2021) 105833. https://doi.org/10.1016/j.nanoen.2021.105833.

[77] K. Zhao, G. Gu, Y. Zhang, B. Zhang, F. Yang, L. Zhao, et al., The self-powered CO2 gas sensor based on gas discharge induced by triboelectric nanogenerator, Nano Energy, 53 (2018) 898-905. https://doi.org/10.1016/j.nanoen.2018.09.057.

[78] H.S. Hong, N.H. Ha, D.D. Thinh, N.H. Nam, N.T. Huong, N. Thi Hue, et al., Enhanced sensitivity of self-powered NO2 gas sensor to sub-ppb level using triboelectric effect based on surface-modified PDMS and 3D-graphene/CNT network, Nano Energy, 87 (2021) 106165. https://doi.org/10.1016/j.nanoen.2021.106165.

[79] X. Xue, Y. Nie, B. He, L. Xing, Y. Zhang, Z.L. Wang, Surface free-carrier screening effect

on the output of a ZnO nanowire nanogenerator and its potential as a self-powered active gas sensor, Nanotechnology, 24 (2013) 225501. https://doi.org/10.1088/0957-4484/24/22/225501.

[80] Y. Lin, P. Deng, Y. Nie, Y. Hu, L. Xing, Y. Zhang, et al., Room-temperature self-powered ethanol sensing of a Pd/ZnO nanoarray nanogenerator driven by human finger movement, Nanoscale, 6 (2014) 4604-10. https://doi.org/10.1039/C3NR06809A.

[81] P. Wang, P. Deng, Y. Nie, Y. Zhao, Y. Zhang, L. Xing, et al., Synthesis of CdS nanorod arrays and their applications in flexible piezo-driven active H2S sensors, Nanotechnology, 25 (2014) 075501. https://doi.org/10.1088/0957-4484/25/7/075501.

[82] W. Zang, Y. Nie, D. Zhu, P. Deng, L. Xing, X. Xue, Core–shell In2O3/ZnO nanoarray nanogenerator as a self-powered active gas sensor with high H2S sensitivity and selectivity at room temperature, The Journal of Physical Chemistry C, 118 (2014) 9209-16. https://doi.org/10.1021/jp500516t.